

Microscopic theory of Brownian motion revisited: The Rayleigh model

Changho Kim and George Em Karniadakis*

Division of Applied Mathematics, Brown University, Providence, Rhode Island 02912, USA

(Received 4 January 2013; published 14 March 2013)

We investigate three force autocorrelation functions $\langle \mathbf{F}(0) \cdot \mathbf{F}(t) \rangle$, $\langle \mathbf{F}^+(0) \cdot \mathbf{F}^+(t) \rangle$, and $\langle \mathbf{F}_0(0) \cdot \mathbf{F}_0(t) \rangle$ and the friction coefficient γ for the Rayleigh model (a massive particle in an ideal gas) by analytic methods and molecular-dynamics (MD) simulations. Here, \mathbf{F} and \mathbf{F}^+ are the total force and the Mori fluctuating force, respectively, whereas \mathbf{F}_0 is the force on the Brownian particle under the frozen dynamics, where the Brownian particle is held fixed and the solvent particles move under the external potential due to the presence of the Brownian particle. By using ensemble averaging and the ray representation approach, we obtain two expressions for $\langle \mathbf{F}_0(0) \cdot \mathbf{F}_0(t) \rangle$ in terms of the one-particle trajectory and corresponding expressions for γ by the time integration of these expressions. Performing MD simulations of the near-Brownian-limit (NBL) regime, we investigate the convergence of $\langle \mathbf{F}(0) \cdot \mathbf{F}(t) \rangle$ and $\langle \mathbf{F}^+(0) \cdot \mathbf{F}^+(t) \rangle$ and compare them with $\langle \mathbf{F}_0(0) \cdot \mathbf{F}_0(t) \rangle$. We show that for a purely repulsive potential between the Brownian particle and a solvent particle, both expressions for $\langle \mathbf{F}_0(0) \cdot \mathbf{F}_0(t) \rangle$ produce $\langle \mathbf{F}^+(0) \cdot \mathbf{F}^+(t) \rangle$ in the NBL regime. On the other hand, for a potential containing an attractive component, the ray representation expression produces only the contribution of the nontrapped solvent particles. However, we show that the net contribution of the trapped particles to γ disappears, and hence we confirm that both the ensemble-averaged expression and the ray representation expression for γ are valid even if the potential contains an attractive component. We also obtain a closed-form expression of γ for the square-well potential. Finally, we discuss theoretical and practical aspects for the evaluation of $\langle \mathbf{F}_0(0) \cdot \mathbf{F}_0(t) \rangle$ and γ .

DOI: [10.1103/PhysRevE.87.032129](https://doi.org/10.1103/PhysRevE.87.032129)

PACS number(s): 05.40.-a

I. INTRODUCTION

While Brownian motion has inspired researchers from various fields of science [1], as a canonical example of stochastic processes, it has also served as an archetypal model in nonequilibrium statistical mechanics. One of the fundamental questions is how the dynamics of Brownian particles can be described without knowing the dynamics of the entire system. The microscopic theory of Brownian motion addresses how mesoscopic equations for the Brownian particles are derived starting from first principles, i.e., without introducing any *a priori* stochastic features to a microscopic system except the concept of an ensemble, and how the parameters of resulting mesoscopic equations are related with the microscopic structure of the system.

In this context, the simplest physical system is arguably a system consisting of a single spherical Brownian particle of mass M surrounded by solvent particles of mass m ; this system has been extensively studied [2]. In the Brownian limit $m \ll M$, the momentum \mathbf{P} of the Brownian particle obeys Langevin's phenomenological equation [3],

$$\dot{\mathbf{P}}(t) = -\frac{\gamma}{M}\mathbf{P}(t) + \mathbf{\Gamma}(t), \quad (1)$$

where γ is the friction coefficient, $\mathbf{\Gamma}(t)$ is d -dimensional Gaussian white noise with noise intensity D , i.e., $\langle \mathbf{\Gamma}(t) \cdot \mathbf{\Gamma}(t') \rangle = dD\delta(t - t')$, and d is the dimension of the space.

A. Microscopic expressions of γ

One of the heuristic scenarios toward Eq. (1) in the Brownian limit can be suggested by the generalized Langevin

equation for \mathbf{P} , which was derived by Mori [4],

$$\dot{\mathbf{P}}(t) = -\frac{1}{M} \int_0^t K(\tau)\mathbf{P}(t - \tau)d\tau + \mathbf{F}^+(t), \quad (2)$$

where $K(t)$ is the Mori memory kernel and $\mathbf{F}^+(t)$ is the corresponding fluctuating force. Assuming that the interaction between the Brownian particle and each solvent particle becomes instantaneous on the time scale of the Brownian particle in the Brownian limit, it is expected that the fluctuating force $\mathbf{F}^+(t)$ exerted on the Brownian particle by the solvent becomes δ -correlated. By the fluctuation-dissipation theorem

$$K(t) = \frac{\beta}{d} \langle \mathbf{F}^+(0) \cdot \mathbf{F}^+(t) \rangle, \quad (3)$$

the memory kernel $K(t)$ also becomes a δ function. Here, β is the inverse temperature of the system and the brackets denote the equilibrium average. Hence, in the near-Brownian-limit (NBL) regime, a Markovian approximation of Eq. (2) due to the large time-scale separation leads to Eq. (1) and γ is approximated by the time integral of $K(t)$, which is equal to

$$\gamma^* = \frac{\beta}{d} \int_0^\infty \langle \mathbf{F}^+(0) \cdot \mathbf{F}^+(t) \rangle dt. \quad (4)$$

There have been similar expressions of the Green-Kubo type, which relate the friction coefficient γ with the time integrals of some force autocorrelation functions. Kirkwood has proposed the following expression [5]:

$$\gamma^* = \frac{\beta}{d} \int_0^{\tau^*} \langle \mathbf{F}(0) \cdot \mathbf{F}(t) \rangle dt, \quad (5)$$

where $\mathbf{F}(t)$ is the total force exerted on the Brownian particle. Since the time integral would vanish if the upper time limit is increased to infinity, a cutoff τ^* is introduced under the assumption that the time integral presents a plateau and its

*george_karniadakis@brown.edu

value does not depend on the precise value of τ^* . It has been demonstrated that the thermodynamic limit, where the number of the solvent particles tends to infinity, is essential for the existence of τ^* [6,7].

Another expression which we also consider in this paper is given from the *frozen dynamics*, where the infinite mass limit $M \rightarrow \infty$ is taken so that the Brownian particle is held fixed and the solvent particles move under the external potential due to the presence of the Brownian particle. Under a certain assumption on the time scales of the bath, Mazur and Oppenheim have performed a detailed analysis [8] to show that in the Brownian limit, the friction coefficient γ is given by

$$\gamma_0 = \frac{\beta}{d} \int_0^\infty \langle \mathbf{F}_0(0) \cdot \mathbf{F}_0(t) \rangle dt, \quad (6)$$

where $\mathbf{F}_0(t)$ is the force exerted on the *fixed* Brownian particle in the frozen dynamics.

In addition, the value of γ can also be estimated from the momentum autocorrelation function in the NBL regime through the relation

$$\langle \mathbf{P}(0) \cdot \mathbf{P}(t) \rangle = \frac{dM}{\beta} e^{-\gamma t/M}, \quad (7)$$

which is derived from Eq. (1).

Molecular-dynamics (MD) simulation studies using these relations and corresponding theories have been extensively performed on the system of a single Brownian particle (or a trace particle with different mass and size) in a simple fluid. However, since MD simulations in the NBL regime require high computational cost, it was not until recently that systematic investigations using long-time and large-size MD simulations were attempted [7,9,10]. Specifically, the increase in computational cost of the MD simulation with smaller mass ratio m/M is not only due to the larger time-scale separation in the system, but also to a larger number of solvent particles that are necessary to satisfy the condition $M \ll Nm$, where N is the number of solvent particles. For this reason, determining a *precise* value of γ from a direct MD simulation approach is not a routine computation of this juncture.

The *primary objective* of this paper is to systematically explore the limiting behavior of the system in the NBL regime. More specifically, the main physical quantities of interest are the total force autocorrelation function $\langle \mathbf{F}(0) \cdot \mathbf{F}(t) \rangle$ and the fluctuating force autocorrelation function $\langle \mathbf{F}^+(0) \cdot \mathbf{F}^+(t) \rangle$ in the NBL regime as well as the frozen dynamics force autocorrelation function $\langle \mathbf{F}_0(0) \cdot \mathbf{F}_0(t) \rangle$. We investigate the convergence of the total force and fluctuating force autocorrelation functions in the Brownian limit and compare them with the frozen dynamics force autocorrelation function. Long-time and large-size MD simulations with carefully chosen MD parameters are performed so that the tails of the force autocorrelation functions are clearly compared and the numerical integration of the force autocorrelation functions provides numerically reliable values. Compared to recent related numerical studies [7,9,10], we use all methods of obtaining the friction coefficient (i.e., the time integration of the three force autocorrelation functions and the decay rate of the momentum autocorrelation function) and adopt

a synergistic approach with analytic methods, which will be described below.

B. Rayleigh model

We introduce the noninteracting bath assumption to our system, which allows us an alternative analytic approach. Under this assumption, no solvent particle interacts with the other solvent particles, and solvent particles interact only with the Brownian particle. Hence, in the frozen dynamics, the dynamics of each solvent particle is decoupled from those of the other solvent particles. This feature enables us to derive analytic expressions for $\langle \mathbf{F}_0(0) \cdot \mathbf{F}_0(t) \rangle$, which are given in terms of a one-particle trajectory. A numerical evaluation of the analytic expression for the frozen dynamics force autocorrelation function allows us to adjust MD simulation parameters. Also, the numerical results with no statistical errors help us to interpret the MD simulation results more clearly. We note that there is a trade-off with the introduction of the noninteracting bath assumption. The system becomes analytically more manageable but it loses some physically interesting features, such as the hydrodynamic effect of the bath [11]. However, the system still legitimately describes a certain physical phenomenon, i.e., Brownian motion in a gaseous medium.

The Rayleigh model (a massive particle in an ideal gas) has been extensively studied with the assumption of elastic collisions. An explicit expression of the friction coefficient γ in the Brownian limit has been derived by various methods [12–15], and the velocity autocorrelation function and the Mori memory kernel in the NBL regime have also been investigated [16]. Mathematically rigorous results have been available for the one-dimensional model with various limiting procedures toward the Brownian limit [17], and some multidimensional extensions [18] and subsequent generalizations to introduce rotational motion to the Brownian particle [19] and to impose a reflecting boundary to the system [20] have followed. Some progress in the generalization of the interaction structure other than elastic collisions and multiple Brownian particles has been recently made by Kusuoka and Liang [21]. The Rayleigh model has also been studied in the context of the adiabatic piston with nonequilibrium conditions [22–26] and the reactive Rayleigh gas [27].

An *equally important objective* of this paper is to comprehensively understand the version of the Rayleigh model where an internal structure of interaction is considered, compared to the version of the Rayleigh model where only elastic collisions are considered. As specific examples, we consider four typical interaction potentials: the hard-sphere (HS) interaction and the square-well (SqW) potential as analytic examples, and the Lennard-Jones (LJ) and Weeks-Chandler-Andersen (WCA) potentials as numerical examples. First, for a general short-ranged interaction potential, we derive two expressions for the force autocorrelation function $\langle \mathbf{F}_0(0) \cdot \mathbf{F}_0(t) \rangle$ of the frozen dynamics and corresponding expressions for the friction coefficient γ . The first one is obtained from the ensemble average, whereas the other is from the time average and is given in terms of the ray representation following Kusuoka and Liang's approach [21]. Then, we apply these results to the four potentials. For the HS interaction and the SqW potential,

closed-form expressions for γ are obtained. For the WCA and LJ potentials, we numerically evaluate the expressions and compare them with the MD simulation results. Based on the results for the four potential cases, theoretical and practical aspects for the evaluation of $\langle \mathbf{F}_0(0) \cdot \mathbf{F}_0(t) \rangle$ and γ are presented.

The rest of the paper is organized as follows. In Sec. II, the system is defined and previous theoretical results are summarized. In Sec. III, the ensemble-averaged expressions for $\langle \mathbf{F}_0(0) \cdot \mathbf{F}_0(t) \rangle$ and γ are derived. In Sec. IV, some relevant portion of Kusuoka and Liang's work is presented with a physical explanation followed by the ray representation expressions for $\langle \mathbf{F}_0(0) \cdot \mathbf{F}_0(t) \rangle$ and γ . In Sec. V, analytic results for the HS interaction and the SqW potential are derived. In Sec. VI, numerical results for the WCA and LJ potentials are presented and discussed. In Sec. VII, we provide a summary with some discussion.

II. SYSTEM AND KNOWN RESULTS

A. System

We consider a system consisting of a single spherical Brownian particle of mass M and a total of N noninteracting solvent particles of mass m . The dimension of the space and the inverse temperature of the system are denoted by d ($d = 2$ or 3) and β , respectively. \mathbf{X} and \mathbf{P} denote the position and momentum of the Brownian particle, respectively, and $\mathbf{x}^N = (\mathbf{x}_1, \mathbf{x}_2, \dots, \mathbf{x}_N)$ and $\mathbf{p}^N = (\mathbf{p}_1, \mathbf{p}_2, \dots, \mathbf{p}_N)$ denote those of the solvent particles. The interaction potential $U(r)$ between the Brownian particle and a solvent is a function of inter-particle distance. We assume that the potential is short-ranged with a cutoff radius R_0 . The Hamiltonian H of the system is written as

$$H = \sum_{n=1}^N \left[\frac{\mathbf{p}_n \cdot \mathbf{p}_n}{2m} + U(|\mathbf{x}_n - \mathbf{X}|) \right] + \frac{\mathbf{P} \cdot \mathbf{P}}{2M}. \quad (8)$$

Although all particles, including the Brownian particle, have point masses and only their translational motions are considered, the form of $U(r)$ may introduce the size of the Brownian particle. That is, for example, for the LJ and WCA potentials with parameters ϵ and σ , we may think that the radius of the Brownian particle is σ .

In the frozen dynamics, the Brownian particle is held fixed at a certain position \mathbf{X} and the solvent particles move under the bath Hamiltonian

$$H_0 = \sum_{n=1}^N \left[\frac{\mathbf{p}_n \cdot \mathbf{p}_n}{2m} + U(|\mathbf{x}_n - \mathbf{X}|) \right]. \quad (9)$$

Since H_0 is the sum of one-particle Hamiltonians, the motion of each solvent particle becomes independent in the frozen dynamics. To distinguish from the frozen dynamics, we refer to the dynamics under the system Hamiltonian H as the *full* dynamics.

We introduce two statistical averages. The *full-system* equilibrium average of a physical quantity θ is defined as

$$\langle \theta \rangle = \int \theta \rho d\mathbf{X} d\mathbf{P} d\mathbf{x}^N d\mathbf{p}^N, \quad (10)$$

where ρ is the equilibrium distribution

$$\rho = e^{-\beta H} / \int e^{-\beta H} d\mathbf{X} d\mathbf{P} d\mathbf{x}^N d\mathbf{p}^N. \quad (11)$$

On the other hand, the *bath* equilibrium average is defined as

$$\langle \theta \rangle_b = \int \theta \rho_b d\mathbf{x}^N d\mathbf{p}^N, \quad (12)$$

where ρ_b is the bath equilibrium distribution

$$\rho_b = e^{-\beta H_0} / \int e^{-\beta H_0} d\mathbf{x}^N d\mathbf{p}^N. \quad (13)$$

Note that the bath equilibrium average can be defined for the full dynamics as well as for the frozen dynamics. For the former case, $\langle \theta \rangle_b$ is a function of \mathbf{X} and \mathbf{P} . If $\langle \theta \rangle_b$ does not depend on \mathbf{X} , $\langle \theta \rangle$ is equal to the average of $\langle \theta \rangle_b$ over the Maxwell distribution of \mathbf{P} . For notational simplicity, we drop the subscript for $\langle \mathbf{F}_0(0) \cdot \mathbf{F}_0(t) \rangle_b$ throughout the paper, i.e., $\langle \mathbf{F}_0(0) \cdot \mathbf{F}_0(t) \rangle \equiv \langle \mathbf{F}_0(0) \cdot \mathbf{F}_0(t) \rangle_b$.

B. Force autocorrelation functions and their time integrals

As stated in Sec. I, three force autocorrelation functions $\langle \mathbf{F}(0) \cdot \mathbf{F}(t) \rangle$, $\langle \mathbf{F}^+(0) \cdot \mathbf{F}^+(t) \rangle$, and $\langle \mathbf{F}_0(0) \cdot \mathbf{F}_0(t) \rangle$ and their time integrals are investigated in this paper. While $\mathbf{F}(t)$ is the force exerted on the Brownian particle in the full dynamics, $\mathbf{F}_0(t)$ is the force in the frozen dynamics. In other words, for the Liouville operators iL and iL_0 corresponding to H and H_0 , respectively, $\mathbf{F}(t) = e^{iL t} \mathbf{F}$ and $\mathbf{F}_0(t) = e^{iL_0 t} \mathbf{F}$. On the other hand, $\mathbf{F}^+(t)$ is defined for the full dynamics through the generalized Langevin equation, Eq. (2). We note that for the theoretical results summarized in this subsection, the noninteracting bath assumption is not necessary.

Before stating the relations of these force autocorrelation functions in the Brownian limit, we specify the limiting procedure toward the Brownian limit to be considered in this section. The infinite mass limit $M \rightarrow \infty$ has been mainly considered in the physics literature. In this limiting procedure, all parameters except the mass M of the Brownian particle are assumed to be fixed. However, as Español and Zúñiga pointed out [6], it has been implicitly assumed that the thermodynamic limit $N \rightarrow \infty$ is taken before the infinite mass limit. This is clearly seen through the relation (see Ref. [6])

$$\langle \mathbf{P} \cdot \mathbf{P} \rangle = \frac{d}{\beta} \frac{MNm}{M + Nm} \equiv \frac{d}{\beta} \mu, \quad (14)$$

which shows that the condition $M \ll Nm$ should be satisfied in order to have $\langle \mathbf{P} \cdot \mathbf{P} \rangle = \beta^{-1} dM$. Hence, we also assume that the condition is valid along the infinite mass limit so that $\mu \approx M$.

In the infinite mass limit, $\langle \mathbf{F}(0) \cdot \mathbf{F}(t) \rangle$ and $\langle \mathbf{F}^+(0) \cdot \mathbf{F}^+(t) \rangle$ coincide. This can be shown by the relation of the Laplace transforms of these force autocorrelation functions (see Ref. [6]),

$$\tilde{C}^+(s) = \tilde{C}(s) \left[1 - \frac{\beta \tilde{C}(s)}{d\mu s} \right]^{-1}, \quad (15)$$

where $\tilde{C}(s)$ and $\tilde{C}^+(s)$ are the Laplace transforms of $C(t) = \langle \mathbf{F}(0) \cdot \mathbf{F}(t) \rangle$ and $C^+(t) = \langle \mathbf{F}^+(0) \cdot \mathbf{F}^+(t) \rangle$, respectively. By

letting $\mu \rightarrow \infty$ (i.e., $M \rightarrow \infty$ after $N \rightarrow \infty$), we see that $\tilde{C}(s)$ and $\tilde{C}^+(s)$ coincide.

Mazur and Oppenheim have investigated the asymptotic form [28] of $\langle \mathbf{F}(0) \cdot \mathbf{F}(t) \rangle$ in the Brownian limit under the assumption that correlation functions which are governed by the frozen dynamics are short-lived [8]. This assumption means that there is a characteristic time τ_b of the bath such that, for $t > \tau_b$,

$$\langle A_0(t_1) e^{iL_0 t_1} B_0(t_2) \rangle_b = \langle A_0(t_1) \rangle_b \langle B_0(t_2) \rangle_b, \quad (16)$$

where $A_0(t_1) = e^{iL_0 t_1} A$ and $B_0(t_2) = e^{iL_0 t_2} B$. By using projection operator techniques [29] with the projection operator $\langle \rangle_b$, they have derived an exact equation for \mathbf{P} , which is different from Eq. (2). For the corresponding fluctuating force $\mathbf{F}_{\text{MO}}^+(t)$, they have shown that $\langle \mathbf{F}_{\text{MO}}^+(0) \cdot \mathbf{F}_{\text{MO}}^+(t) \rangle_b$ has a well-behaved series expansion in powers of the mass ratio m/M with $\langle \mathbf{F}_0(0) \cdot \mathbf{F}_0(t) \rangle$, the lowest-order term. They have also obtained an asymptotic form of $\langle \mathbf{F}(0) \cdot \mathbf{F}(t) \rangle_b$, containing a slowly decaying contribution proportional to $M^{-1} e^{-\gamma_0 t/M}$. By taking the Maxwellian average to $\langle \mathbf{F}(0) \cdot \mathbf{F}(t) \rangle_b$, we have the same form for $\langle \mathbf{F}(0) \cdot \mathbf{F}(t) \rangle$,

$$\langle \mathbf{F}(0) \cdot \mathbf{F}(t) \rangle \approx \langle \mathbf{F}_0(0) \cdot \mathbf{F}_0(t) \rangle - \frac{d\gamma_0^2}{\beta M} e^{-\gamma_0 t/M}. \quad (17)$$

We note that from Eq. (17) it can be shown that $\int_0^\infty \langle \mathbf{F}(0) \cdot \mathbf{F}(t) \rangle dt = 0$.

Under the same assumption for the time scale τ_b , Hynes *et al.* have shown that the autocorrelation function of the Mori fluctuating force $\mathbf{F}^+(t)$ has the following form [30]:

$$\langle \mathbf{F}^+(0) \cdot \mathbf{F}^+(t) \rangle = \frac{dM}{\beta} [i\Omega_{11}(t) + \Delta_{11}(t)]. \quad (18)$$

The first term $\beta^{-1} dM i\Omega_{11}(t)$ is equal to the Maxwellian average of the Mazur-Oppenheim fluctuating force autocorrelation function $\langle \mathbf{F}_{\text{MO}}^+(0) \cdot \mathbf{F}_{\text{MO}}^+(t) \rangle_b$ and thus it has a well-behaved series expansion. On the other hand, the second term $\beta^{-1} dM \Delta_{11}(t)$ is proportional to $M^{-3} e^{-3\gamma_0 t/M}$. The exponential decay term, however, does not change the behavior of the time integral significantly in this case, because its contribution to γ^+ in Eq. (4) is $O(M^{-2})$. Therefore, in the Brownian limit, $\langle \mathbf{F}^+(0) \cdot \mathbf{F}^+(t) \rangle$ and its time integral γ^+ converge to $\langle \mathbf{F}_0(0) \cdot \mathbf{F}_0(t) \rangle$ and γ_0 (i.e., γ), respectively.

III. ENSEMBLE-AVERAGED EXPRESSIONS FOR $\langle \mathbf{F}_0(0) \cdot \mathbf{F}_0(t) \rangle$ AND γ

As discussed in Sec. II B, the frozen dynamics force autocorrelation function $\langle \mathbf{F}_0(0) \cdot \mathbf{F}_0(t) \rangle$ provides the asymptotic form [28] of $\langle \mathbf{F}^+(0) \cdot \mathbf{F}^+(t) \rangle$ in the Brownian limit and its time integral is equal to γ . In this section, under the noninteracting bath assumption, we derive ensemble-averaged expressions for $\langle \mathbf{F}_0(0) \cdot \mathbf{F}_0(t) \rangle$ and γ , which are expressed by one-particle ensemble-averaged quantities.

A. Expression for $\langle \mathbf{F}_0(0) \cdot \mathbf{F}_0(t) \rangle$

Since $\langle \mathbf{F}_0(0) \cdot \mathbf{F}_0(t) \rangle$ does not depend on the fixed position of the Brownian particle, we assume that the Brownian particle is fixed at the origin. We denote the force exerted on a solvent particle located at \mathbf{x} by $\mathbf{f}(\mathbf{x})$, i.e., $\mathbf{f}(\mathbf{x}) = -U'(|\mathbf{x}|) \frac{\mathbf{x}}{|\mathbf{x}|}$.

For the solvent with initial configuration $\{\mathbf{x}^N, \mathbf{p}^N\}$, the net force $\mathbf{F}_0(0)$ exerted on the Brownian particle by the solvent is given as $-\sum_{i=1}^N \mathbf{f}(\mathbf{x}_i)$. Likewise, $\mathbf{F}_0(t) = -\sum_{i=1}^N \mathbf{f}(\mathbf{x}_i(t))$, where $\mathbf{x}_i(t) = e^{iL_0 t} \mathbf{x}_i$. Then, we have the following form:

$$\langle \mathbf{F}_0(0) \cdot \mathbf{F}_0(t) \rangle = N \langle \mathbf{f}(\mathbf{x}_1) \cdot \mathbf{f}(\mathbf{x}_1(t)) \rangle_b. \quad (19)$$

The cross terms $\langle \mathbf{f}(\mathbf{x}_i) \cdot \mathbf{f}(\mathbf{x}_j(t)) \rangle_b$ with $i \neq j$ disappeared in Eq. (19), since \mathbf{x}_i and $\mathbf{x}_j(t)$ are independent and $\langle \mathbf{f}(\mathbf{x}_i) \rangle_b = 0$ by the symmetry of ρ_b . The average with respect to ρ_b can be reduced to the average with respect to one-particle Boltzmann distribution. With the subscript 1 dropped, Eq. (19) is expressed as follows:

$$\langle \mathbf{F}_0(0) \cdot \mathbf{F}_0(t) \rangle = \frac{N}{V^*} \int d\mathbf{p} \phi(\mathbf{p}) I(\mathbf{p}, t), \quad (20)$$

where V is the volume of the system and

$$I(\mathbf{p}, t) = \int_V d\mathbf{x} e^{-\beta U(|\mathbf{x}|)} \mathbf{f}(\mathbf{x}) \cdot \mathbf{f}(\mathbf{x}(t)), \quad (21a)$$

$$\phi(\mathbf{p}) = \left(\frac{\beta}{2\pi m} \right)^{d/2} e^{-\frac{\beta}{2m} \mathbf{p} \cdot \mathbf{p}}, \quad (21b)$$

$$V^* = \int_V d\mathbf{x} e^{-\beta U(|\mathbf{x}|)}. \quad (21c)$$

As expected, $\langle \mathbf{F}_0(0) \cdot \mathbf{F}_0(t) \rangle$ is proportional to the number density of the solvent. We note that for a sufficiently large value of V and a short-ranged potential $U(r)$, $N/V \approx N/V^*$.

Since the interaction potential U is a function of the interparticle distance with cutoff R_0 , Eq. (20) can be further simplified. For $d = 2$, by introducing new variables r, θ, u , and ϕ , we parametrize $\mathbf{x} = (r \cos \theta, r \sin \theta)$ and $\mathbf{p} = (u \cos(\theta + \phi), u \sin(\theta + \phi))$. Then, $\mathbf{f}(\mathbf{x}) \cdot \mathbf{f}(\mathbf{x}(t))$ is a function of r, u , and ϕ , but does not depend on θ . Also, for ϕ and $-\phi$, $\mathbf{f}(\mathbf{x}) \cdot \mathbf{f}(\mathbf{x}(t))$ has the same value. Hence, we obtain

$$\langle \mathbf{F}_0(0) \cdot \mathbf{F}_0(t) \rangle = \frac{2a\beta}{m} \int_0^\infty du \int_0^\pi d\phi \int_0^{R_0} dr \times e^{-\beta[\frac{u^2}{2m} + U(r)]} r u \mathbf{f}(\mathbf{x}) \cdot \mathbf{f}(\mathbf{x}(t)), \quad (22)$$

where a is the number density of the solvent particles and $\mathbf{f}(\mathbf{x}) \cdot \mathbf{f}(\mathbf{x}(t))$ is calculated for $\mathbf{x} = (r, 0)$ and $\mathbf{p} = (u \cos \phi, u \sin \phi)$. Similarly, for $d = 3$, we obtain

$$\langle \mathbf{F}_0(0) \cdot \mathbf{F}_0(t) \rangle = 8\pi^2 a \left(\frac{\beta}{2\pi m} \right)^{3/2} \int_0^\infty du \int_0^\pi d\phi \int_0^{R_0} dr \times e^{-\beta[\frac{u^2}{2m} + U(r)]} r^2 u^2 \sin \phi \mathbf{f}(\mathbf{x}) \cdot \mathbf{f}(\mathbf{x}(t)). \quad (23)$$

Note that since the trajectory under $U(r)$ is on a plane, we can use the same function $\mathbf{f}(\mathbf{x}) \cdot \mathbf{f}(\mathbf{x}(t))$ as $d = 2$.

B. Expression for γ

From Eqs. (6) and (20), we can obtain an expression for γ . Since $\int_0^t \mathbf{f}(\mathbf{x}(s)) ds = \mathbf{p}(t) - \mathbf{p}$, we have

$$\gamma = \frac{a\beta}{d} \lim_{t \rightarrow \infty} \int d\mathbf{p} \phi(\mathbf{p}) \int_V d\mathbf{x} e^{-\beta U(|\mathbf{x}|)} \mathbf{f}(\mathbf{x}) \cdot [\mathbf{p}(t) - \mathbf{p}]. \quad (24)$$

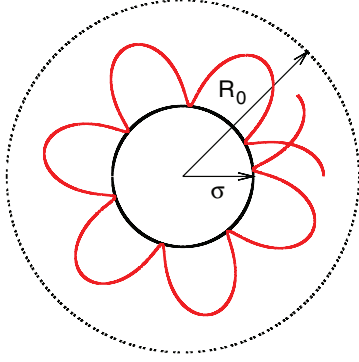


FIG. 1. (Color online) A typical trajectory of a solvent particle trapped in the well of the (truncated) LJ potential is depicted by the red line. The solid circle of radius σ indicates the Brownian particle, whereas the dotted circle of radius $R_0 = 2.5\sigma$ indicates the interaction range.

For a purely repulsive potential, $\mathbf{p}_\infty = \lim_{t \rightarrow \infty} \mathbf{p}(t)$ is always well-defined, since every trajectory quickly leaves the interaction range and the momentum no longer changes after it leaves the interaction range. Hence, we can take the limit $t \rightarrow \infty$ inside by replacing $\mathbf{p}(t)$ with \mathbf{p}_∞ . For a potential containing an attractive component, however, some trajectories are trapped in the potential well and the corresponding solvent particles interact with the Brownian particle forever and \mathbf{p}_∞ is not well-defined. For the LJ potential, for example, if

$$\frac{|\mathbf{p}|^2}{2m} + U(|\mathbf{x}|) = \frac{|\mathbf{p}_\perp|^2}{2m} \frac{|\mathbf{x}|^2}{r_*^2} + U(r_*), \quad (25)$$

where \mathbf{p}_\perp is defined so that $\mathbf{p} = \mathbf{p}_\parallel + \mathbf{p}_\perp$ and $\mathbf{x} \cdot \mathbf{p}_\perp = 0$ has a root r_* in the interval $(|\mathbf{x}|, R_0)$, the particle cannot escape from the potential well; see Fig. 1. However, we can show that the net contribution of the trapped particles to γ disappears. The ensemble average of the product of $\mathbf{f}(\mathbf{x})$ and $\mathbf{p}(t)$ over the trapped particles becomes decoupled as t tends to infinity so that it shrinks to zero. Also, the ensemble average of $\mathbf{f}(\mathbf{x}) \cdot \mathbf{p}$ over the trapped particles is zero by the time-reversal property. Hence, we obtain

$$\gamma = \frac{a\beta}{d} \iint_{\text{nontrapped}} d\mathbf{x} d\mathbf{p} \phi(\mathbf{p}) e^{-\beta U(|\mathbf{x}|)} \mathbf{f}(\mathbf{x}) \cdot (\mathbf{p}_\infty - \mathbf{p}). \quad (26)$$

As we did in Sec. III A, Eq. (26) is further simplified; for $d = 2$,

$$\gamma = \frac{a\beta^2}{m} \int_0^\infty du \int_0^\pi d\phi \int_0^{R_0} dr \times e^{-\beta[\frac{u^2}{2m} + U(r)]} r u \mathbb{I}(\mathbf{x}, \mathbf{p}) \mathbf{f}(\mathbf{x}) \cdot (\mathbf{p}_\infty - \mathbf{p}), \quad (27)$$

and for $d = 3$,

$$\gamma = \frac{8}{3} \pi^2 a \beta \left(\frac{\beta}{2\pi m} \right)^{3/2} \int_0^\infty du \int_0^\pi d\phi \int_0^{R_0} dr \times e^{-\beta[\frac{u^2}{2m} + U(r)]} r^2 u^2 \sin \phi \mathbb{I}(\mathbf{x}, \mathbf{p}) \mathbf{f}(\mathbf{x}) \cdot (\mathbf{p}_\infty - \mathbf{p}), \quad (28)$$

where $\mathbb{I}(\mathbf{x}, \mathbf{p}) = 0$ if the trajectory is trapped and it is equal to 1 otherwise.

IV. RAY REPRESENTATION APPROACH

In this section, an alternative method of studying the microscopic theory of Brownian motion is discussed and then applied to obtain a microscopic formula for the frozen dynamics force autocorrelation function. It was devised for the Rayleigh model, and microscopic formulas for the friction coefficient γ and the noise intensity D have been derived in terms of the ray representation by Kusuoka and Liang [21]. Instead of considering the ensemble of the solvent and taking the ensemble average (as we did in Sec. III), they have obtained their results by time-averaging for a given realization of the initial solvent configuration. For mathematical convenience, some restrictive assumptions on the interaction potential and the initial solvent configuration have been made. Under these assumptions, for a sufficiently small mass ratio m/M , every incoming solvent particle penetrates the Brownian particle. However, the penetration of solvent particles into the Brownian particle is not valid for our solid Brownian particle case. Specifically, neither the interaction potentials we consider in this paper nor the Boltzmann distribution satisfies the assumptions. Here we discuss and examine the validity of the ray representation approach beyond the original Kusuoka and Liang's assumptions [21].

Specifically, in this section, we use a different limiting procedure from the infinite mass limit, which has been used in Kusuoka and Liang's work. Roughly speaking, we consider $m \rightarrow 0$ rather than $M \rightarrow \infty$ to achieve the Brownian limit $m/M \rightarrow 0$. Since the momentum of the Brownian particle obeys the Ornstein-Uhlenbeck process *without* scaling under this limit, this limit is more favorable for presenting mathematically rigorous statements and proofs; it has also been used in Refs. [18–20]. However, we can also use the infinite mass limit with the ray representation approach, and the main results under the infinite mass limit are presented below in Sec. IV F.

We first present some relevant parts of Kusuoka and Liang's work with an emphasis on physical meaning. In Sec. IV A, a system and a limiting procedure to be considered in this section are introduced. The ray representation and the adiabatic trajectory are explained in Secs. IV B and IV C, respectively. In Sec. IV D, Kusuoka and Liang's result for the noise intensity D is presented in a heuristic way. Then, we derive a microscopic expression for the frozen dynamics force autocorrelation function in Sec. IV E. In Sec. IV F, we present the expressions for $\langle \mathbf{F}_0(0) \cdot \mathbf{F}_0(t) \rangle$ and γ under the infinite mass limit with further simplified forms.

A. System description

We consider a Brownian particle of mass M surrounded by an infinite number of solvent particles of mass m in d -dimensional space ($d = 2$ or 3). The position and velocity of the Brownian particle at time t are denoted by $\mathbf{X}(t)$ and $\mathbf{V}(t)$, respectively, while the positions and velocities of the solvent particles are denoted by $\mathbf{x}_i(t)$ and $\mathbf{v}_i(t)$, respectively, with $i = 1, 2, \dots$. The Brownian particle interacts with each solvent particle via a short-ranged interaction potential U , but there is no interaction between the solvent particles. We further assume that the interaction potential is a function of

the interparticle distance between the Brownian particle and a solvent particle, i.e., $U = U(r)$, and that the potential has a cutoff R_0 , i.e., $U(|\mathbf{X} - \mathbf{x}_i|) = 0$ if $|\mathbf{X} - \mathbf{x}_i| > R_0$. We use the notation $\nabla U(\mathbf{x}) = U'(|\mathbf{x}|) \frac{\mathbf{x}}{|\mathbf{x}|}$ for $\mathbf{x} \in \mathbb{R}^d$.

Since the total energy of the system is given as

$$\frac{1}{2}M|\mathbf{V}|^2 + \sum_i \left(\frac{1}{2}m|\mathbf{v}_i|^2 + U(|\mathbf{x}_i - \mathbf{X}|) \right),$$

the equations of motion for the Brownian particle are given as

$$\dot{\mathbf{X}}(t) = \mathbf{V}(t), \quad (29a)$$

$$\dot{\mathbf{V}}(t) = -\frac{1}{M} \sum_i \nabla U[\mathbf{X}(t) - \mathbf{x}_i(t)]. \quad (29b)$$

Note that the sum is over all solvent particles, but it actually contains a finite number of particles at each time since $U(r)$ is a short-ranged potential. On the other hand, the equations of motion for each solvent particle are given as

$$\dot{\mathbf{x}}_i(t) = \mathbf{v}_i(t), \quad (30a)$$

$$\dot{\mathbf{v}}_i(t) = -\frac{1}{m} \nabla U[\mathbf{x}_i(t) - \mathbf{X}(t)]. \quad (30b)$$

The only randomness we introduce to the system is the initial conditions of the solvent particles. While the initial conditions for the Brownian particle, i.e., $\mathbf{X}(0) = \mathbf{X}_0$ and $\mathbf{V}(0) = \mathbf{V}_0$, are deterministic, the initial configuration of the solvent particles in the $2d$ -dimensional (\mathbf{x}, \mathbf{v}) space is given by the Poisson field with intensity

$$\lambda(d\mathbf{x}, d\mathbf{v}) = \frac{a}{\sqrt{m}} e^{-\beta U(|\mathbf{x} - \mathbf{x}_0|)} \left(\frac{m\beta}{2\pi} \right)^{d/2} e^{-\frac{1}{2}\beta m|\mathbf{v}|^2} d\mathbf{x} d\mathbf{v}, \quad (31)$$

where a is introduced as a density parameter and β is the inverse temperature of the solvent. The number of the particles that are found in the volume element $d\mathbf{x} d\mathbf{v}$ obeys the Poisson distribution with mean $\lambda(d\mathbf{x}, d\mathbf{v})$ and is independent of those in other nonoverlapping volume elements. By integrating λ over \mathbf{v} , we see that the number density of the solvent particles beyond the interaction range of the Brownian particle has mean a/\sqrt{m} . In turn, by integrating λ over \mathbf{x} , we see that the velocity distribution of the solvent particles obeys the Maxwell-Boltzmann distribution. Hence, the initial solvent configuration obtained from the Poisson field is a realization of the solvent configuration in equilibrium.

The Brownian limit we consider in this section is achieved by decreasing m to zero with M fixed. Meanwhile, we fix the parameters a and β and the interaction potential $U(r)$. As we see in Eq. (31), however, as the Brownian limit is achieved, the system contains a larger number of solvent particles in a unit volume and the solvent particles become lighter and faster. In other words, as m goes to zero, the velocities of the solvent particles increase like $O(1/\sqrt{m})$ and so does the number density of the solvent.

Comparison of the two settings considered in Secs. II A and IV A follows. Two different settings of the systems (i.e., a finite number of solvent particles in a finite volume versus an infinite number of solvent particles in a whole space) do not make any essential difference, if sufficiently large values of N

and V are used in the previous setting and the number densities of the solvent particles are the same. On the other hand, the two limiting procedures are not equivalent and result in Langevin equations with different values of γ and D . To derive the Langevin equation from the infinite mass limit considered in the previous section, the momentum \mathbf{P} and time t need to be scaled. For the limiting procedure considered in this section, no scaling is required. However, we note that a system with a nonzero mass ratio $m/M \ll 1$ can be interpreted by either of the two limiting procedures.

In the rest of Sec. IV, we assume that the interaction potential is purely repulsive. In this case, every solvent particle interacts with the Brownian particle for a finite time and then leaves the interaction range. On the other hand, if the potential contains an attractive component, some solvent particles are trapped in the potential well and it is less likely for them to escape from the well as the mass ratio m/M has a smaller value. Some comments for this case are made in this section if necessary, but the overall discussion takes place in Sec. VI.

B. Ray representation

The initial conditions of the solvent particles can be equivalently expressed by the ray representation. This is based on the observation that every incoming solvent particle undergoes a free motion until it interacts with the Brownian particle. Hence, its trajectory can be labeled as a corresponding free motion—a ray.

For a solvent particle with initial position \mathbf{x} and initial velocity \mathbf{v} at time $t = 0$, we consider free motion $\mathbf{x} + t\mathbf{v}$. We denote \bar{t} as the time when the position becomes the closest to the origin and $\bar{\mathbf{x}}$ as the position of the particle at this moment; see Fig. 2. Hence, the scalar \bar{t} and vector $\bar{\mathbf{x}}$ satisfy

$$\mathbf{v} \cdot (\mathbf{x} + \bar{t}\mathbf{v}) = 0, \quad (32a)$$

$$\bar{\mathbf{x}} = \mathbf{x} + \bar{t}\mathbf{v}. \quad (32b)$$

Note that \bar{t} may have a negative value. Also, since \mathbf{v} increases like $O(1/\sqrt{m})$ as $m \rightarrow 0$, we introduce the normalized velocity

$$\bar{\mathbf{v}} = \sqrt{m}\mathbf{v}. \quad (33)$$

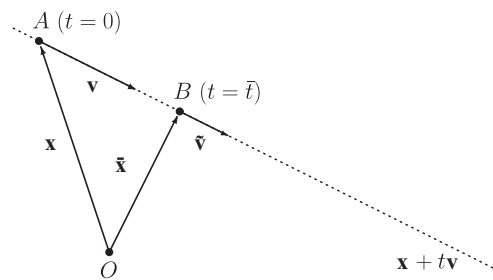


FIG. 2. Schematic diagram for the ray representation. The dotted line indicates the trajectory of free motion of a particle with initial position \mathbf{x} (point A) and initial velocity \mathbf{v} at time $t = 0$, which is parametrized by $\mathbf{x} + t\mathbf{v}$. The ray representation of (\mathbf{x}, \mathbf{v}) is given by $(\bar{t}, \bar{\mathbf{x}}, \bar{\mathbf{v}})$, where $\bar{\mathbf{x}}$ is the closest point (point B) on the line to the origin O (i.e., $\bar{\mathbf{x}} \perp \mathbf{v}$), \bar{t} is the time when the particle arrives at $\bar{\mathbf{x}}$ (i.e., $\mathbf{x} + \bar{t}\mathbf{v} = \bar{\mathbf{x}}$), and $\bar{\mathbf{v}}$ is the normalized velocity of \mathbf{v} (i.e., $\bar{\mathbf{v}} = \sqrt{m}\mathbf{v}$).

Then, our ray representation of (\mathbf{x}, \mathbf{v}) is given as $(\bar{t}, \bar{\mathbf{x}}, \bar{\mathbf{v}})$. We note that bar notation is used for ray representation, whereas a tilde is used to indicate that a variable is scaled.

There is a one-to-one correspondence between the two representations, i.e., between (\mathbf{x}, \mathbf{v}) with $\mathbf{v} \neq 0$ and $(\bar{t}, \bar{\mathbf{x}}, \bar{\mathbf{v}})$ with $\bar{\mathbf{v}} \neq 0$ and $\bar{\mathbf{v}} \cdot \bar{\mathbf{x}} = 0$. For $\bar{\mathbf{v}} \neq 0$, we define $E_{\bar{\mathbf{v}}}$ to be the hyperplane perpendicular to $\bar{\mathbf{v}}$, i.e., $E_{\bar{\mathbf{v}}} = \{\bar{\mathbf{x}} : \bar{\mathbf{v}} \cdot \bar{\mathbf{x}} = 0\}$. Due to the constraint, the dimension of $E_{\bar{\mathbf{v}}}$ is $d - 1$. We denote a volume element on $E_{\bar{\mathbf{v}}}$ by $d\bar{\mathbf{x}}$. We also define a $(2d - 1)$ -dimensional space

$$E = \{(\bar{\mathbf{x}}, \bar{\mathbf{v}}) : \bar{\mathbf{v}} \neq 0, \bar{\mathbf{x}} \cdot \bar{\mathbf{v}} = 0\}. \quad (34)$$

We note that the volume element $d\bar{\mathbf{x}}$ in $E_{\bar{\mathbf{v}}}$ and the space E appear in the microscopic formulas for the noise intensity D and the autocorrelation function of \mathbf{F}_0 ; see Eqs. (53) and (60).

From the ray representation of the initial solvent configuration, one can approximate the times when each solvent particle interacts with the Brownian particle, which is advantageous for our problem. If a solvent particle with ray representation $(\bar{t}, \bar{\mathbf{x}}, \bar{\mathbf{v}})$ interacts with the Brownian particle, the interaction time is approximated as \bar{t} and this approximation becomes more accurate as m has a smaller value. To see this clearly, we introduce a region centered at the origin, which is assumed to be bounded but sufficiently large so that the Brownian particle moves within the region; see Fig. 3. Since the solvent is an ideal gas, the solvent particle undergoes free motion until it enters the interaction range of the Brownian particle. We denote the time interval when the free motion $\mathbf{x} + t\bar{\mathbf{v}}/\sqrt{m}$ stays in the region by $(\bar{t} - \epsilon_1, \bar{t} + \epsilon_2)$, and the time interval when the solvent particle interacts with the Brownian particle by $(t^*, t^* + \epsilon_3)$. Clearly, t^* is contained in $(\bar{t} - \epsilon_1, \bar{t} + \epsilon_2)$, and ϵ_i ($i = 1, 2, 3$) are $O(\sqrt{m})$. Hence, we can approximately consider that the interaction occurs at time \bar{t} with a short duration of order \sqrt{m} . Note that this argument is heuristic

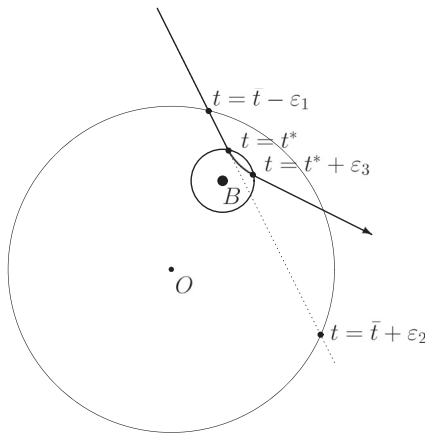


FIG. 3. A typical trajectory of a solvent particle that interacts with the Brownian particle. Point O denotes the origin of the space, while the solid circle B denotes the Brownian particle. The smaller circle indicates the interaction range of the Brownian particle while the larger circle indicates some bounded region containing the origin and the Brownian particle. For a solvent particle with its ray representation $(\bar{t}, \bar{\mathbf{x}}, \bar{\mathbf{v}})$, we denote the times when the free motion $\mathbf{x} + t\bar{\mathbf{v}}/\sqrt{m}$ (drawn by the dotted line) enters and exits the region by $\bar{t} - \epsilon_1$ and $\bar{t} + \epsilon_2$, respectively, and the times when the particle enters and exits the interaction range by t^* and $t^* + \epsilon_3$, respectively.

and it implicitly assumes that the Brownian particle moves much more slowly than the solvent particles and that each solvent particle interacts with the Brownian particle at most once, which is valid for a small value of m .

Now we express the Poisson field for the initial configuration of the solvent in terms of the ray representation. Since we can label the initial configuration of the solvent particles by $\{(x_i, v_i)\}$, we can also express it in terms of the ray representation, i.e., $\{(\bar{t}_i, \bar{\mathbf{x}}_i, \bar{\mathbf{v}}_i)\}$. We define $N(d\bar{t}, d\bar{\mathbf{x}}, d\bar{\mathbf{v}})$ as the corresponding Poisson field on $(\bar{t}, \bar{\mathbf{x}}, \bar{\mathbf{v}})$ space, and we want to find its intensity $\bar{\lambda}(d\bar{t}, d\bar{\mathbf{x}}, d\bar{\mathbf{v}})$. We assume that the initial position of the Brownian particle is at the origin, i.e., $\mathbf{X}_0 = 0$. For sufficiently small m , if a solvent particle is initially positioned inside the interaction range (i.e., $|\mathbf{x}| \leq R_0$), then it leaves the interaction range in a very short time and then no longer affects the movement of the Brownian particle. Thus, if we are interested in a long-time average, the initial solvent configuration near the Brownian particle does not need to be imposed precisely. We approximate $\lambda(d\mathbf{x}, d\mathbf{v})$ in Eq. (31) by the following intensity $\lambda_0(d\mathbf{x}, d\mathbf{v})$:

$$\lambda_0(d\mathbf{x}, d\mathbf{v}) = \frac{a}{\sqrt{m}} \left(\frac{m\beta}{2\pi} \right)^{d/2} e^{-\frac{1}{2}\beta m |\mathbf{v}|^2} d\mathbf{x} d\mathbf{v}. \quad (35)$$

Note that λ_0 is the intensity of the Poisson field for a free ideal gas since $U(r) = 0$ everywhere in this case. Since $\bar{\mathbf{v}} d\bar{t} \perp d\bar{\mathbf{x}}$ and $\mathbf{v} = m^{-1/2}\bar{\mathbf{v}}$, we can express the volume elements

$$d\mathbf{x} = \frac{1}{\sqrt{m}} |\bar{\mathbf{v}}| d\bar{\mathbf{x}} d\bar{t}, \quad (36a)$$

$$d\mathbf{v} = m^{-d/2} d\bar{\mathbf{v}}, \quad (36b)$$

and thus we obtain the intensity of the Poisson field

$$\bar{\lambda}(d\bar{t}, d\bar{\mathbf{x}}, d\bar{\mathbf{v}}) = \frac{a}{m} \left(\frac{\beta}{2\pi} \right)^{d/2} e^{-\frac{1}{2}\beta |\bar{\mathbf{v}}|^2} |\bar{\mathbf{v}}| d\bar{t} d\bar{\mathbf{x}} d\bar{\mathbf{v}}. \quad (37)$$

Note that Eq. (37) is obtained from Eq. (35) rather than Eq. (31). For a purely repulsive potential, the difference between the initial configurations near the Brownian particle only for the initial time, the duration of which is of the order of \sqrt{m} . On the other hand, if the interaction potential has an attractive component, a particle initially located inside the potential well may be trapped depending on its initial velocity and stay for an infinite time as m tends to zero. Hence, in this case, a different initial configuration may cause different dynamics of the Brownian particle for a long time. Thus, we should treat the contribution of those particles precisely and may not approximate $\lambda(d\mathbf{x}, d\mathbf{v})$ by $\lambda_0(d\mathbf{x}, d\mathbf{v})$.

Since $N(d\bar{t}, d\bar{\mathbf{x}}, d\bar{\mathbf{v}})$ is a random discrete measure concentrated on $\{(\bar{t}_i, \bar{\mathbf{x}}_i, \bar{\mathbf{v}}_i)\}$, an integral with respect to $N(d\bar{t}, d\bar{\mathbf{x}}, d\bar{\mathbf{v}})$ is interpreted as follows:

$$\int_{(0, t] \times E} N(d\bar{u}, d\bar{\mathbf{x}}, d\bar{\mathbf{v}}) A(\bar{u}, \bar{\mathbf{x}}, \bar{\mathbf{v}}) = \sum_{0 < \bar{t}_i \leq t} A(\bar{t}_i, \bar{\mathbf{x}}_i, \bar{\mathbf{v}}_i). \quad (38)$$

Its compensated field is denoted by $N_0(d\bar{t}, d\bar{\mathbf{x}}, d\bar{\mathbf{v}})$, i.e.,

$$N_0(d\bar{t}, d\bar{\mathbf{x}}, d\bar{\mathbf{v}}) = N(d\bar{t}, d\bar{\mathbf{x}}, d\bar{\mathbf{v}}) - \bar{\lambda}(d\bar{t}, d\bar{\mathbf{x}}, d\bar{\mathbf{v}}). \quad (39)$$

C. Adiabatic trajectory ψ

As discussed in Sec. IV B, if the system is near the Brownian limit, a solvent particle interacts with the Brownian particle for a very short time. An adiabatic approximation is considered in order to estimate how this instantaneous collision affects the motion of the Brownian particle. In other words, while the Brownian particle interacts with a certain solvent particle, we assume that its position does not change, and we observe the motion of the solvent particle. Then, the equations of motion of the solvent particle are decoupled from those of the other solvent particles.

For a solvent particle with its ray representation $(\bar{t}, \bar{\mathbf{x}}, \bar{\mathbf{v}})$, the interaction occurs near time $t = \bar{t}$ and its duration is $O(\sqrt{m})$. Hence, we introduce a scaled time

$$\bar{s} = \frac{t - \bar{t}}{\sqrt{m}}. \quad (40)$$

We also assume that the Brownian particle is held fixed while the interaction occurs, i.e., $\mathbf{X}(\bar{s}) = \mathbf{X}(\bar{t})$. The adiabatic trajectory $\psi(\bar{s}) = \psi(\bar{s}; \bar{\mathbf{x}}, \bar{\mathbf{v}}, \mathbf{X}(\bar{t}))$ of the solvent particle satisfies

$$\frac{d^2}{d\bar{s}^2} \psi(\bar{s}) = -\nabla U[\psi(\bar{s}) - \mathbf{X}(\bar{t})]. \quad (41)$$

The initial conditions of Eq. (41) are given by the fact that before the particle enters the interaction range (i.e., \bar{s} has a sufficiently large negative value), it satisfies

$$\psi(\bar{s}) = \bar{\mathbf{x}} + \bar{s}\bar{\mathbf{v}}. \quad (42)$$

Under the adiabatic assumption, the total impulse exerted on the Brownian particle during the interaction is given as

$$\mathbf{A}(\bar{t}, \bar{\mathbf{x}}, \bar{\mathbf{v}}) = \sqrt{m} \int_{-\infty}^{\infty} \nabla U[\psi(\bar{s}; \bar{\mathbf{x}}, \bar{\mathbf{v}}, \mathbf{X}(\bar{t})) - \mathbf{X}(\bar{t})] d\bar{s}. \quad (43)$$

We note that the actual integration is over a finite time interval when the particle stays in the interaction range.

D. Noise intensity D

Now we approximate the random force exerted on the Brownian particle. The underlying idea is as follows. In the Brownian limit, a solvent particle with its ray representation $(t, \bar{\mathbf{x}}, \bar{\mathbf{v}})$ interacts with the Brownian particle instantaneously at time t . The impulse exerted on the Brownian particle by the solvent particle is approximated by $\mathbf{A}(t, \bar{\mathbf{x}}, \bar{\mathbf{v}})$. We approximate the force exerted on the Brownian particle at time t by the sum of δ impulses (occurring at time t) having intensity $\mathbf{A}(t, \bar{\mathbf{x}}, \bar{\mathbf{v}})$.

By defining

$$\mathbf{H}(t) = \int_{(0,t] \times E} N(du, d\bar{\mathbf{x}}, d\bar{\mathbf{v}}) \mathbf{A}(u, \bar{\mathbf{x}}, \bar{\mathbf{v}}), \quad (44)$$

we approximate the time integral of the random force exerted on the Brownian particle up to time t . Hence, the random force itself is approximated by the (formal) time derivative of $\mathbf{H}(t)$, i.e.,

$$\mathbf{F}^\delta(t) = \dot{\mathbf{H}}(t), \quad (45)$$

where we used superscript δ to emphasize that the force consists of the sum of δ peaks by its definition. We can show that in the Brownian limit, the quadratic variation of

$\mathbf{H}(t)$ is deterministic (i.e., independent of the realization of the initial solvent configuration) and it grows linearly with time. However, in order to obtain an expression for the slope of the quadratic variation versus time, it suffices to calculate $\mathbb{E}[|\mathbf{H}(t)|^2]$, where $\mathbb{E}[\cdot]$ denotes the expectation over the initial solvent configurations.

We decompose $\mathbf{H}(t)$ into $\mathbf{H}_0(t) + \mathbf{H}_1(t)$, where

$$\mathbf{H}_0(t) = \int_{(0,t] \times E} N_0(du, d\bar{\mathbf{x}}, d\bar{\mathbf{v}}) \mathbf{A}(u, \bar{\mathbf{x}}, \bar{\mathbf{v}}), \quad (46a)$$

$$\mathbf{H}_1(t) = \int_{(0,t] \times E} \bar{\lambda}(du, d\bar{\mathbf{x}}, d\bar{\mathbf{v}}) \mathbf{A}(u, \bar{\mathbf{x}}, \bar{\mathbf{v}}). \quad (46b)$$

Due to the symmetry properties of the potential U and the intensity $\bar{\lambda}$, we have $\mathbf{H}_1(t) = 0$ and thus $\mathbf{H}(t) = \mathbf{H}_0(t)$. By the Itô isometry, we have

$$\mathbb{E}[|\mathbf{H}(t)|^2] = \int_{(0,t] \times E} \bar{\lambda}(du, d\bar{\mathbf{x}}, d\bar{\mathbf{v}}) \mathbb{E}[|\mathbf{A}(u, \bar{\mathbf{x}}, \bar{\mathbf{v}})|^2]. \quad (47)$$

We note that the dependencies on m of \mathbf{A} (proportional to \sqrt{m}) and $\bar{\lambda}$ (proportional to m^{-1}) cancel in Eq. (47); the latter equation can be further simplified. The time dependence of $\mathbf{A}(u, \bar{\mathbf{x}}, \bar{\mathbf{v}})$ is only through the position $\mathbf{X}(u)$ of the Brownian particle, and the integral

$$\int_E \bar{\lambda}(u, d\bar{\mathbf{x}}, d\bar{\mathbf{v}}) |\mathbf{A}(u, \bar{\mathbf{x}}, \bar{\mathbf{v}})|^2$$

does not depend on $\mathbf{X}(u)$ due to the translational invariance of $\bar{\lambda}$. Thus, it is a constant with respect to u . Hence, we may evaluate it with the assumption that the Brownian particle is at the origin. By introducing

$$\tilde{\mathbf{A}}(\bar{\mathbf{x}}, \bar{\mathbf{v}}) = \int_{-\infty}^{\infty} \nabla U(\psi(\bar{s}; \bar{\mathbf{x}}, \bar{\mathbf{v}}, 0)) d\bar{s}, \quad (48)$$

$\mathbb{E}[|\mathbf{A}(u, \bar{\mathbf{x}}, \bar{\mathbf{v}})|^2]$ is replaced by $m|\tilde{\mathbf{A}}(\bar{\mathbf{x}}, \bar{\mathbf{v}})|^2$ in Eq. (47), and we obtain from Eq. (37)

$$\mathbb{E}[|\mathbf{H}(t)|^2] = dDt, \quad (49)$$

where

$$D = \frac{a}{d} \left(\frac{\beta}{2\pi} \right)^{d/2} \int_E |\tilde{\mathbf{A}}(\bar{\mathbf{x}}, \bar{\mathbf{v}})|^2 e^{-\frac{1}{2}\beta|\bar{\mathbf{v}}|^2} |\bar{\mathbf{v}}| d\bar{\mathbf{x}} d\bar{\mathbf{v}}. \quad (50)$$

By comparing Eq. (49) with the relation

$$\mathbb{E}[|\mathbf{H}(t)|^2] = \int_0^t du \int_0^t du' \mathbb{E}[\mathbf{F}^\delta(u) \cdot \mathbf{F}^\delta(u')], \quad (51)$$

we have

$$\mathbb{E}[\mathbf{F}^\delta(t) \cdot \mathbf{F}^\delta(t')] = dD\delta(t - t'), \quad (52)$$

which means that D is actually the noise intensity of \mathbf{F}^δ . Equation (50) can be written as follows:

$$D = \frac{a}{d} \int_E \left| \int_{-\infty}^{\infty} \nabla U(\psi(\bar{s}; \bar{\mathbf{x}}, \bar{\mathbf{v}}, 0)) d\bar{s} \right|^2 \bar{\rho}(\bar{\mathbf{x}}, \bar{\mathbf{v}}) d\bar{\mathbf{x}} d\bar{\mathbf{v}}, \quad (53)$$

where

$$\bar{\rho}(\bar{\mathbf{x}}, \bar{\mathbf{v}}) = \left(\frac{\beta}{2\pi} \right)^{d/2} e^{-\frac{1}{2}\beta|\bar{\mathbf{v}}|^2} |\bar{\mathbf{v}}|. \quad (54)$$

Hence, D is expressed as the average of the square of the total momentum change after each collision over the rays with weight $\bar{\rho}$.

As mentioned above, the quadratic variation of $\mathbf{H}(t)$ is dDt in the Brownian limit and D is obtained from this relation. Hence, for each initial solvent configuration, *almost surely*, we can obtain D from the time average, which means that the use of the expectation $\mathbb{E}[\cdot]$ is not essential.

E. Time-averaged expression for $\langle \mathbf{F}_0(0) \cdot \mathbf{F}_0(\bar{\tau}) \rangle$

For a small value of $m \ll M$, the frozen dynamics force autocorrelation function has a time scale of order \sqrt{m} . By using the tilde notation $\bar{\tau}$ for microscopic time, we denote the autocorrelation function by $\langle \mathbf{F}_0(0) \cdot \mathbf{F}_0(\bar{\tau}) \rangle$. As we did in Sec. IV D, we derive a microscopic expression for $\langle \mathbf{F}_0(0) \cdot \mathbf{F}_0(\bar{\tau}) \rangle$ by taking the time average of $\mathbb{E}[\mathbf{F}_0(t) \cdot \mathbf{F}_0(t + \bar{\tau})]$, i.e.,

$$\langle \mathbf{F}_0(0) \cdot \mathbf{F}_0(\bar{\tau}) \rangle = \lim_{T \rightarrow \infty} \frac{1}{T} \int_0^T \mathbb{E}[\mathbf{F}_0(t) \cdot \mathbf{F}_0(t + \bar{\tau})] dt. \quad (55)$$

Since $\mathbf{F}_0(t)$ is the sum of the forces exerted by the colliding solvent particles at time t , i.e., $\mathbf{F}_0(t) = -\sum_i \mathbf{f}_i(t)$, $\mathbf{F}_0(t) \cdot \mathbf{F}_0(t + \bar{\tau})$ is decomposed into two parts:

$$\mathbf{F}_0(t) \cdot \mathbf{F}_0(t + \bar{\tau}) = I_1 + I_2, \quad (56)$$

where I_1 contains the overlap of the forces of the same particle, i.e., $\sum_i \mathbf{f}_i(t) \cdot \mathbf{f}_i(t + \bar{\tau})$, and I_2 contains the overlap of the forces of different particles, i.e., $\sum_i \sum_{i \neq j} \mathbf{f}_i(t) \cdot \mathbf{f}_j(t + \bar{\tau})$. For a colliding particle with ray representation $(t, \bar{\mathbf{x}}, \bar{\mathbf{v}})$, the total overlap between the force and its translation by time $\bar{\tau}$ is given in terms of the following function:

$$\tilde{B}(\bar{\tau}, \bar{\mathbf{x}}, \bar{\mathbf{v}}) = \int_{-\infty}^{\infty} \nabla U(\boldsymbol{\psi}(\bar{s}; \bar{\mathbf{x}}, \bar{\mathbf{v}}, 0)) \cdot \nabla U(\boldsymbol{\psi}(\bar{s} + \bar{\tau}; \bar{\mathbf{x}}, \bar{\mathbf{v}}, 0)) d\bar{s}. \quad (57)$$

In other words, we have

$$I_1 dt = m \int_E N(dt, d\bar{\mathbf{x}}, d\bar{\mathbf{v}}) \tilde{B}(\bar{\tau}, \bar{\mathbf{x}}, \bar{\mathbf{v}}), \quad (58)$$

and thus, by Eqs. (37) and (54), we obtain

$$\mathbb{E}[I_1] = a \int_E \tilde{B}(\bar{\tau}, \bar{\mathbf{x}}, \bar{\mathbf{v}}) \bar{\rho}(\bar{\mathbf{x}}, \bar{\mathbf{v}}) d\bar{\mathbf{x}} d\bar{\mathbf{v}}. \quad (59)$$

On the other hand, by the independence of two colliding particles and the isotropy of $\bar{\lambda}$, we have $\mathbb{E}[I_2] = 0$. Therefore, $\mathbb{E}[\mathbf{F}_0(t) \cdot \mathbf{F}_0(t + \bar{\tau})] = \mathbb{E}[I_1]$ is *stationary* and we obtain the following expression for $\langle \mathbf{F}_0(0) \cdot \mathbf{F}_0(\bar{\tau}) \rangle$:

$$\langle \mathbf{F}_0(0) \cdot \mathbf{F}_0(\bar{\tau}) \rangle = a \int_E \tilde{B}(\bar{\tau}, \bar{\mathbf{x}}, \bar{\mathbf{v}}) \bar{\rho}(\bar{\mathbf{x}}, \bar{\mathbf{v}}) d\bar{\mathbf{x}} d\bar{\mathbf{v}}. \quad (60)$$

Now we show that Kusuoka and Liang's microscopic expression [21], Eq. (53), can be derived from Eq. (60) by using Mazur and Oppenheim's result [8]. From Eq. (6) and the fluctuation-dissipation relation $D\beta = 2\gamma$, we have

$$D = \frac{2}{d} \int_0^{\infty} \langle \mathbf{F}_0(0) \cdot \mathbf{F}_0(\bar{\tau}) \rangle d\bar{\tau}. \quad (61)$$

Since

$$2 \int_0^{\infty} \tilde{B}(\bar{\tau}, \bar{\mathbf{x}}, \bar{\mathbf{v}}) d\bar{\tau} = \left| \int_{-\infty}^{\infty} \nabla U(\boldsymbol{\psi}(\bar{s}; \bar{\mathbf{x}}, \bar{\mathbf{v}}, 0)) d\bar{s} \right|^2, \quad (62)$$

we retrieve Eq. (53) from Eqs. (60) and (61).

We also discuss the validity of Eq. (60). Since $\bar{\rho}$ is obtained from $\bar{\lambda}$ and, in turn, $\bar{\lambda}$ is obtained from λ_0 rather than λ , the validity of the expression depends on whether λ is correctly approximated by λ_0 . As we discussed in Sec. IV B, for a purely repulsive potential, the difference of the initial configurations near the Brownian particle does not affect the long-time dynamics and thus the approximation is valid. On the other hand, for a potential containing an attractive component, we cannot neglect the initially trapped particles, which will stay in the potential well forever in the frozen dynamics. Clearly, the contribution of such particles is not considered in Eq. (60) since their trajectories cannot be expressed by the adiabatic trajectory $\boldsymbol{\psi}$, which describes a solvent particle entering and then leaving the potential range. Actually, $\langle \mathbf{F}_0(0) \cdot \mathbf{F}_0(\bar{\tau}) \rangle$ in Eq. (60) contains only the contribution of the incoming solvent particles, and it results from the Poisson field whose intensity is given as follows:

$$\lambda_1(d\mathbf{x}, d\mathbf{v}) = \lambda_0(d\mathbf{x}, d\mathbf{v}) \mathbb{I}(\mathbf{x}), \quad (63)$$

where $\mathbb{I}(\mathbf{x}) = 1$ if $|\mathbf{x}| > R_0$ and $\mathbb{I}(\mathbf{x}) = 0$ otherwise. Note that if $\lambda_1(d\mathbf{x}, d\mathbf{v})$ is assumed for the Poisson field, then there is no trapped particle in the frozen dynamics.

F. Results under the infinite mass limit

We present the ray representation results under the infinite mass limit, which is considered in Secs. II and III. For the ray representation, we use momentum \mathbf{p} instead of velocity. For $(\bar{\mathbf{x}}, \mathbf{p}) \in E$, where $E = \{(\bar{\mathbf{x}}, \mathbf{p}) \in \mathbb{R}^{2d} : \bar{\mathbf{x}} \cdot \mathbf{p} = 0, \mathbf{p} \neq 0\}$, we define the adiabatic trajectory $\boldsymbol{\psi}(t) = \boldsymbol{\psi}(t; \bar{\mathbf{x}}, \mathbf{p})$ satisfying

$$m\boldsymbol{\psi}''(t) = -\nabla U(\boldsymbol{\psi}(t)) \quad (64)$$

and $\boldsymbol{\psi}(t) = \bar{\mathbf{x}} + \frac{t}{m}\mathbf{p}$ for sufficiently negatively large t (i.e., before the particle enters the interaction range). The expression for the frozen dynamics force autocorrelation function is given as

$$\langle \mathbf{F}_0(0) \cdot \mathbf{F}_0(\tau) \rangle = a \int_E B(\tau, \bar{\mathbf{x}}, \mathbf{p}) \bar{\rho}(\bar{\mathbf{x}}, \mathbf{p}) d\bar{\mathbf{x}} d\mathbf{p}, \quad (65)$$

where a is the number density of the solvent particles,

$$B(\tau, \bar{\mathbf{x}}, \mathbf{p}) = \int_{-\infty}^{\infty} \nabla U(\boldsymbol{\psi}(t)) \cdot \nabla U(\boldsymbol{\psi}(t + \tau)) dt, \quad (66a)$$

$$\bar{\rho}(\bar{\mathbf{x}}, \mathbf{p}) = \left(\frac{\beta}{2\pi m} \right)^{d/2} \frac{|\mathbf{p}|}{m} e^{-\frac{\beta}{2m} |\mathbf{p}|^2}. \quad (66b)$$

The expression for the friction coefficient is given as

$$\gamma = \frac{a\beta}{2d} \int_E |\mathbf{p}_{\infty} - \mathbf{p}|^2 \bar{\rho}(\bar{\mathbf{x}}, \mathbf{p}) d\bar{\mathbf{x}} d\mathbf{p}, \quad (67)$$

where $\mathbf{p}_{\infty} = m \lim_{t \rightarrow \infty} \boldsymbol{\psi}'(t)$.

Since the interaction potential U is a function of interparticle distance, Eqs. (65) and (67) can be further simplified. For $d = 2$, $\bar{\mathbf{x}}$ and \mathbf{p} can be parametrized as follows: $\bar{\mathbf{x}} = (-r \sin \phi, r \cos \phi)$ and $\mathbf{p} = (u \cos \phi, u \sin \phi)$ with

$u > 0$, $0 \leq \phi < 2\pi$, $-R_0 \leq r \leq R_0$. Since $B(\tau, \bar{\mathbf{x}}, \mathbf{p})$ does not depend on ϕ , we introduce

$$B_0(\tau, r, u) = B(\tau, \bar{\mathbf{x}}_0, \mathbf{p}_0), \quad (68)$$

where $\bar{\mathbf{x}}_0 = (0, r)$ and $\mathbf{p}_0 = (u, 0)$, and we integrate Eq. (65) over ϕ to obtain in the two-dimensional case

$$\langle \mathbf{F}_0(0) \cdot \mathbf{F}_0(\tau) \rangle = \frac{2a\beta}{m^2} \int_0^\infty du \int_0^{R_0} dr e^{-\frac{\beta}{2m}u^2} u^2 B_0(\tau, r, u). \quad (69)$$

We also used the fact that $B_0(\tau, -r, u) = B_0(\tau, r, u)$. Likewise, for $d = 3$, we have

$$\langle \mathbf{F}_0(0) \cdot \mathbf{F}_0(\tau) \rangle = \frac{8\pi^2 a}{m} \left(\frac{\beta}{2\pi m} \right)^{3/2} \int_0^\infty du \int_0^{R_0} dr \times e^{-\frac{\beta}{2m}u^2} r u^3 B_0(\tau, r, u). \quad (70)$$

Note that a $(2d - 1)$ -dimensional integration in Eq. (65) is reduced to two-dimensional integrations in Eqs. (69) and (70). Similarly, we obtain simplified expressions for γ ; for $d = 2$,

$$\gamma = \frac{a\beta^2}{2m^2} \int_0^\infty du \int_0^{R_0} dr e^{-\frac{\beta}{2m}u^2} u^2 |\mathbf{p}_\infty - \mathbf{p}|^2, \quad (71)$$

and for $d = 3$,

$$\gamma = \frac{4\pi^2 a\beta}{3m} \left(\frac{\beta}{2\pi m} \right)^{3/2} \int_0^\infty du \int_0^{R_0} dr e^{-\frac{\beta}{2m}u^2} r u^3 |\mathbf{p}_\infty - \mathbf{p}|^2. \quad (72)$$

V. ANALYTIC RESULTS

In this section, we derive analytic expressions of γ for the HS interaction and the SqW potential and show that the ensemble-averaged expression, Eq. (26), and the ray representation expression, Eq. (67), produce identical results for each potential. For the numerical values of γ for these potentials and the comparison with the WCA and LJ potential, see Figs. 15 and 16. The HS interaction has parameter R as the radius of the Brownian particle; when the interparticle distance between a solvent particle and the Brownian particle becomes R , an elastic collision occurs. The SqW potential we consider has the following form:

$$U_{\text{SqW}}(r) = \begin{cases} \infty & \text{if } r < R_1, \\ -\epsilon & \text{if } R_1 < r < R_2, \\ 0 & \text{if } r > R_2. \end{cases} \quad (73)$$

The closed-form expression of γ for the three-dimensional HS system, Eq. (77), has been derived in the following: in Ref. [12] by the generalized Fokker-Planck equation, by the calculation of the distribution of changes of momentum of the Brownian particle, and by the Kirkwood formula; in Ref. [13] by the density expansion of the momentum autocorrelation function; and in Ref. [14], by the Boltzmann equation. An equivalent expression under the limiting procedure considered in Sec. IV has been derived by a mathematically rigorous probabilistic method [18].

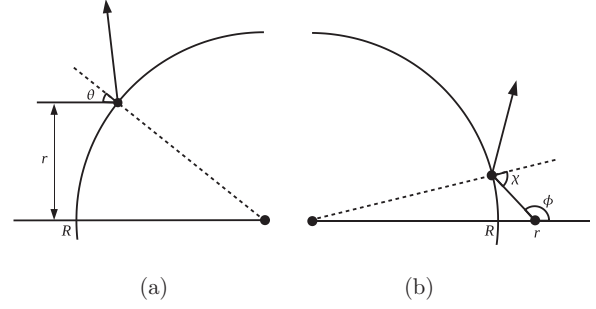


FIG. 4. Some variables used in the calculation of γ of the HS system for (a) the ray representation approach and (b) the ensemble average.

A. HS interaction

1. Ray representation

For $d = 2$, we use Eq. (71) and consider a particle with $\bar{\mathbf{x}} = (0, r)$ and $\mathbf{p} = (u, 0)$. For nonzero $\mathbf{p}_\infty - \mathbf{p}$, it suffices to consider $0 \leq r \leq R$. By introducing the angle θ , which satisfies $\sin \theta = \frac{r}{R}$ [see Fig. 4(a)], we express the magnitude of momentum change as follows:

$$|\mathbf{p}_\infty - \mathbf{p}| = 2u \cos \theta. \quad (74)$$

From Eq. (71), we have

$$\gamma = \frac{2aR\beta^2}{m^2} \int_0^{\pi/2} d\theta \int_0^\infty du u^4 \cos^3 \theta e^{-\frac{\beta}{2m}u^2}, \quad (75)$$

and thus

$$\gamma = 2aR \sqrt{\frac{2\pi m}{\beta}}. \quad (76)$$

Similarly, for $d = 3$, from Eqs. (72) and (74) we obtain

$$\gamma = \frac{8}{3} a R^2 \sqrt{\frac{2\pi m}{\beta}}. \quad (77)$$

2. Ensemble average

In Eqs. (27) and (28), $\mathbf{f}(\mathbf{x}) \cdot (\mathbf{p}_\infty - \mathbf{p})$ is nonzero only when $r = R$. To express this as a δ function, we only need to consider $r \geq R$. To have a collision with the wall, the angle ϕ should be in the range of $[\pi - \arcsin \frac{R}{r}, \pi]$. The angle of incidence is denoted by χ , which satisfies $\sin \chi = \frac{r}{R} \sin \phi$; see Fig. 4(b). The time Δt that it takes for the particle to hit the wall is expressed as follows:

$$\Delta t = - \left(\cos \chi + \frac{r}{R} \cos \phi \right) \frac{mR}{u}. \quad (78)$$

By denoting the momentum change after the collision by $\Delta \mathbf{p}$, we have

$$\mathbf{f}(\mathbf{x}(t)) = \Delta \mathbf{p} \delta(t - \Delta t), \quad (79)$$

$$\mathbf{p}(t) = \mathbf{p} + \Delta \mathbf{p} H(t - \Delta t), \quad (80)$$

where $H(t)$ is the Heaviside step function, and thus

$$\mathbf{f}(\mathbf{x}) \cdot (\mathbf{p}_\infty - \mathbf{p}) = |\Delta \mathbf{p}|^2 \delta(\Delta t) H(\Delta t). \quad (81)$$

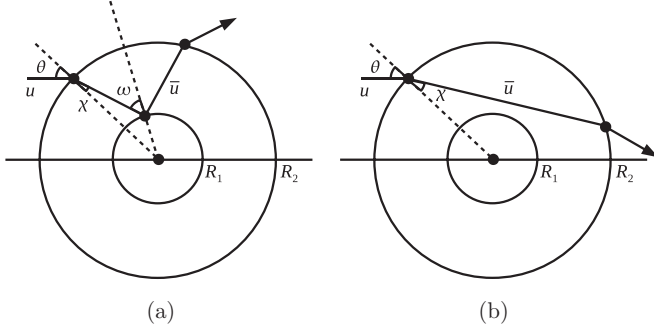


FIG. 5. Two cases to be considered in the calculation of γ for the SqW system by the ray representation approach. Panel (a) corresponds to the case $(\theta, u) \in \mathcal{D}_1$, whereas panel (b) corresponds to $(\theta, u) \in \mathcal{D}_2$.

To have an instantaneous collision (i.e., $\Delta t = 0$), the limit $r \rightarrow R$ with $\frac{\pi}{2} \leq \phi \leq \pi$ is considered, which leads to $\chi \rightarrow \pi - \phi$. Since $\frac{\partial \Delta t}{\partial r} = -\frac{m}{u \cos \phi}$ and $|\Delta \mathbf{p}| = -2u \cos \phi$ under the limit, we obtain

$$\mathbf{f}(\mathbf{x}) \cdot (\mathbf{p}_\infty - \mathbf{p}) = -\frac{4}{m} u^3 \cos^3 \phi \delta(r - R) H(r - R). \quad (82)$$

Hence, for $d = 2$, by introducing $\theta = \pi - \phi$, we obtain the identical integral for γ to Eq. (75) and thus the identical result to Eq. (76). Similarly, for $d = 3$, we obtain Eq. (77) from Eqs. (28) and (82).

B. SqW potential

1. Ray representation

Since we only need to consider $0 \leq r < R_2$, we introduce the angle of incidence to the outer wall, θ , which satisfies $\sin \theta = \frac{r}{R_2}$; see Fig. 5. We also denote the angle of refraction and the magnitude of refracted momentum by χ and \bar{u} , respectively, which satisfy

$$\frac{1}{2m} \bar{u}^2 - \epsilon = \frac{1}{2m} u^2, \quad (83a)$$

$$\bar{u} \sin \chi = u \sin \theta. \quad (83b)$$

The condition $\sin \chi < \frac{R_1}{R_2}$ is equivalent to the condition that the refracted particle collides with the inner wall. Hence, when $\sin \theta < \frac{R_1}{R_2}$, the particle hits the inner wall for all $u > 0$. If $\sin \theta > \frac{R_1}{R_2}$, we define

$$u_* = \frac{R_1 \sqrt{2m\epsilon}}{\sqrt{R_2^2 \sin^2 \theta - R_1^2}}. \quad (84)$$

If $u < u_*$, the particle hits the inner wall, otherwise the particle passes through the interaction range without colliding with the inner wall. Hence, we calculate the integral

$$\gamma = \frac{a R_2 \beta^2}{2m^2} \int_0^{\frac{\pi}{2}} d\theta \int_0^\infty du u^2 \cos \theta e^{-\frac{\beta}{2m} u^2} |\mathbf{p}_\infty - \mathbf{p}|^2 \quad (85)$$

by dividing the domain into \mathcal{D}_1 and \mathcal{D}_2 defined as follows:

$$\mathcal{D}_1 = \left\{ 0 \leq \theta < \arcsin \frac{R_1}{R_2}, u > 0 \right\} \cup \left\{ \arcsin \frac{R_1}{R_2} < \theta < \frac{\pi}{2}, 0 < u < u_* \right\}, \quad (86a)$$

$$\mathcal{D}_2 = \left\{ \arcsin \frac{R_1}{R_2} < \theta < \frac{\pi}{2}, u > u_* \right\}. \quad (86b)$$

For the case of a collision with the inner wall [i.e., for $(\theta, u) \in \mathcal{D}_1$], we denote the angle of incidence on the inner wall by ω [see Fig. 5 (a)], which satisfies

$$\sin \omega = \frac{R_2}{R_1} \sin \chi. \quad (87)$$

We also denote the momentum changes after refraction, reflection, and subsequent refraction by $\Delta \mathbf{p}_1$, $\Delta \mathbf{p}_2$, and $\Delta \mathbf{p}_3$, respectively. Then, the total momentum change is given as $\mathbf{p}_\infty - \mathbf{p} = \Delta \mathbf{p}_1 + \Delta \mathbf{p}_2 + \Delta \mathbf{p}_3$, and we have

$$|\Delta \mathbf{p}_1| = |\Delta \mathbf{p}_3| = \bar{u} \cos \chi - u \cos \theta \equiv A(u, \theta), \quad (88a)$$

$$|\Delta \mathbf{p}_2| = 2\bar{u} \cos \omega \equiv B(u, \theta), \quad (88b)$$

$$\Delta \mathbf{p}_1 \cdot \Delta \mathbf{p}_2 = \Delta \mathbf{p}_2 \cdot \Delta \mathbf{p}_3 = -A(u, \theta) B(u, \theta) \cos(\omega - \chi), \quad (88c)$$

$$\Delta \mathbf{p}_1 \cdot \Delta \mathbf{p}_3 = A^2(u, \theta) \cos 2(\omega - \chi). \quad (88d)$$

Note that we defined A and B as functions of u and θ since other variables such as \bar{u} , χ , and ω are functions of u and θ . Then, for $(\theta, u) \in \mathcal{D}_1$, we have

$$|\mathbf{p}_\infty - \mathbf{p}|^2 = 2A^2[1 + \cos 2(\omega - \chi)] - 4AB \cos(\omega - \chi) + B^2. \quad (89)$$

For the case of no collision with the inner wall, the momentum changes $\Delta \mathbf{p}_1$ and $\Delta \mathbf{p}_2$ after two sequential refractions satisfy

$$|\Delta \mathbf{p}_1| = |\Delta \mathbf{p}_2| = A(u, \theta), \quad (90a)$$

$$\Delta \mathbf{p}_1 \cdot \Delta \mathbf{p}_2 = -A^2(u, \theta) \cos 2\chi. \quad (90b)$$

Hence, for $(\theta, u) \in \mathcal{D}_2$, we have

$$|\mathbf{p}_\infty - \mathbf{p}|^2 = 2A^2[1 - \cos 2\chi]. \quad (91)$$

By combining the results for two cases, we obtain a formula for γ as the sum of two integrals defined in Eqs. (85) and (86). The expressions for $|\mathbf{p}_\infty - \mathbf{p}|^2$ are given in Eqs. (89) and (91). The explicit expressions for the intermediate variables as functions of u and θ are given as follows:

$$A(u, \theta) = \sqrt{u^2 \cos^2 \theta + 2m\epsilon} - u \cos \theta, \quad (92a)$$

$$B(u, \theta) = 2\sqrt{\left(1 - \frac{R_2^2}{R_1^2} \sin^2 \theta\right) u^2 + 2m\epsilon}, \quad (92b)$$

$$\cos(\omega - \chi) = \frac{B(u, \theta) \sqrt{u^2 \cos^2 \theta + 2m\epsilon}}{2(u^2 + 2m\epsilon)} + \frac{R_2 u^2 \sin^2 \theta}{R_1 (u^2 + 2m\epsilon)}, \quad (92c)$$

$$1 - \cos 2\chi = \frac{2u^2 \sin^2 \theta}{u^2 + 2m\epsilon}. \quad (92d)$$

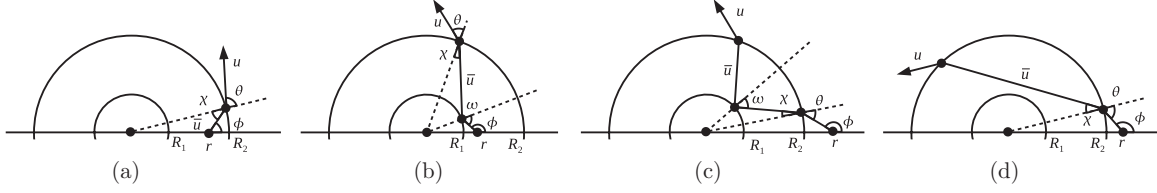


FIG. 6. Four cases to be considered in the calculation of γ for the SqW system by using the ensemble-averaged expression. Panels (a), (b), (c), and (d) correspond to the limits E1, E2, E3, and E4, respectively, in the text.

2. Ensemble average

For instantaneous collisions of nontrapped particles, we consider the following limits:

(E1) $r \rightarrow R_2 - 0$ with $0 \leq \phi \leq \frac{\pi}{2}$.

(E2) $r \rightarrow R_1 + 0$ with $\frac{\pi}{2} \leq \phi \leq \pi$.

(E3) $r \rightarrow R_2 + 0$ with $\frac{\pi}{2} \leq \phi \leq \pi$ (with collision with the inner wall).

(E4) $r \rightarrow R_2 + 0$ with $\frac{\pi}{2} \leq \phi \leq \pi$ (without collision with the inner wall).

To use the expressions we obtained in the ray representation calculation, we use u as the magnitude of the momentum outside the potential range and \bar{u} as the one inside the potential range. Hence, the magnitude of the initial momentum is denoted by \bar{u} in cases E1 and E2, whereas it is denoted by u in cases E3 and E4. Also, the angles of incidence and refraction when the particle passes through the outer wall from inside are denoted by χ and θ , respectively. If the particle hits the inner wall, the angle of incidence is denoted by ω . For the definition of those variables in each case, see Fig. 6.

Since the particle is initially located inside the potential range in cases E1 and E2, there are minima $\bar{u}_*^{(1)}$ and $\bar{u}_*^{(2)}$ for the magnitude of the initial momentum in order for the particle to escape from the interaction range for the two cases. Under the limits E1 and E2, they are given as

$$\bar{u}_*^{(1)} = \frac{\sqrt{2m\epsilon}}{\cos \phi}, \quad (93a)$$

$$\bar{u}_*^{(2)} = \sqrt{\frac{2m\epsilon}{1 - \frac{R_1^2}{R_2^2} \sin^2 \phi}}. \quad (93b)$$

On the other hand, under the limits E3 and E4, the angle of incidence θ becomes $\pi - \phi$. For $(\theta, u) \in \mathcal{D}_1$, there is a collision with the inner wall (i.e., belonging to case E3), whereas there is no collision (i.e., E4) for $(\theta, u) \in \mathcal{D}_2$.

In case E1, the magnitude of momentum change $\Delta \mathbf{p}_1$ after the refraction is given as

$$|\Delta \mathbf{p}_1| = A(u, \theta), \quad (94)$$

and thus we have

$$\mathbf{f}(\mathbf{x}) \cdot (\mathbf{p}_\infty - \mathbf{p}) = \frac{1}{m} \bar{u} \cos \phi \delta(r - R_2) H(R_2 - r) |\Delta \mathbf{p}_1|^2. \quad (95)$$

The contribution of case (E1) to the integral for γ is given as

$$\gamma^{(1)} = \frac{aR_2\beta^2}{2m^2} \int_0^{\frac{\pi}{2}} d\chi \int_{\bar{u}_*^{(1)}}^\infty d\bar{u} \bar{u}^2 \cos \chi A^2(u, \theta) e^{-\beta[\frac{\bar{u}^2}{2m} - \epsilon]}, \quad (96)$$

and by the change of variables from (χ, \bar{u}) to (θ, u) we have

$$\gamma^{(1)} = \frac{aR_2\beta^2}{2m^2} \int_0^{\frac{\pi}{2}} d\theta \int_0^\infty du u^2 \cos \theta A^2(u, \theta) e^{-\frac{\beta}{2m}u^2}. \quad (97)$$

For the other cases, we can similarly express each contribution to γ by an integral for θ and u :

$$\gamma^{(k)} = \frac{aR_2\beta^2}{2m^2} \iint_{\mathcal{D}^{(k)}} d\theta du u^2 \cos \theta e^{-\frac{\beta}{2m}u^2} I^{(k)}, \quad (98)$$

where $\mathcal{D}^{(1)} = \mathcal{D}_1 \cup \mathcal{D}_2$, $\mathcal{D}^{(2)} = \mathcal{D}^{(3)} = \mathcal{D}_1$, $\mathcal{D}^{(4)} = \mathcal{D}_2$,

$$I^{(1)} = A^2, \quad (99a)$$

$$I^{(2)} = B^2 - 2AB \cos(\omega - \chi), \quad (99b)$$

$$I^{(3)} = A^2[1 + 2 \cos 2(\omega - \chi)] - 2AB \cos(\omega - \chi), \quad (99c)$$

$$I^{(4)} = A^2[1 - 2 \cos 2\chi]. \quad (99d)$$

Therefore, we obtain the identical expression for $\gamma = \gamma^{(1)} + \gamma^{(2)} + \gamma^{(3)} + \gamma^{(4)}$ to the ray representation approach.

VI. NUMERICAL RESULTS

A. MD setup

For the LJ and WCA potentials, we perform two-dimensional NVE molecular-dynamics simulations for the full dynamics to observe the convergence of the total force autocorrelation function and the fluctuating force autocorrelation function in the Brownian limit. In other words, we numerically obtain force autocorrelation functions $\langle \mathbf{F}(0) \cdot \mathbf{F}(\tilde{\tau}) \rangle_{\text{NBL}}$ and $\langle \mathbf{F}^+(0) \cdot \mathbf{F}^+(\tilde{\tau}) \rangle_{\text{NBL}}$ in the near-Brownian-limit (NBL) regime, which are defined as follows:

$$\langle \mathbf{F}(0) \cdot \mathbf{F}(\tilde{\tau}) \rangle = \langle \mathbf{F}(0) \cdot \mathbf{F}(\tilde{\tau}) \rangle_{\text{NBL}} + O\left(\frac{m}{M}\right), \quad (100a)$$

$$\langle \mathbf{F}^+(0) \cdot \mathbf{F}^+(\tilde{\tau}) \rangle = \langle \mathbf{F}^+(0) \cdot \mathbf{F}^+(\tilde{\tau}) \rangle_{\text{NBL}} + O\left(\frac{m}{M}\right), \quad (100b)$$

where $\tilde{\tau}$ is the microscopic time defined as t/\sqrt{m} . These two functions are introduced for numerical purposes, but we do not claim that the rate of convergence in Eq. (100) is uniform for all time scales. We also perform the corresponding frozen dynamics simulations to obtain the frozen dynamics force autocorrelation function $\langle \mathbf{F}_0(0) \cdot \mathbf{F}_0(\tilde{\tau}) \rangle$ and then compare the

MD simulation results with the results evaluated from the analytic expressions.

The system parameters for the MD simulations are defined as follows. The mass of a solvent particle is set as $m = 0.01$ and the number of the solvent particles is set as $N = 10^4$. The simulation domain is a square with side $L = 100$ and periodic boundary conditions are imposed. For the full dynamics, the mass M of the Brownian particle is increased from $M = 0.01$ to 1. Note that N is chosen sufficiently large so that $\frac{M}{Nm} \leq 0.01$. The temperature of the system is defined in terms of the average kinetic energy of the system and the inverse temperature is given as $\beta = 1$. For the interaction potential between the Brownian particle and a solvent particle, the WCA potential with parameters $\sigma = 1$ and $\epsilon = 1$ (cutoff $R_0 = 2^{1/6}\sigma$) is chosen for a purely repulsive potential and the LJ potential with parameters $\sigma = 1$ and $\epsilon = 1$ (cutoff $R_0 = 2.5\sigma$) is chosen for a potential with an attractive component. All results are given in reduced units with ϵ the unit of energy, σ the unit of length, and M the unit of mass.

The Brownian particle is initially located at the origin. The initial positions of the solvent particles are chosen randomly so that they are distributed uniformly outside the interaction range of the Brownian particle. The velocities of the solvent particles are chosen from the Maxwell-Boltzmann distribution. The time integration is performed by the velocity Verlet algorithm with time step size $\Delta t = 10^{-4}$. The temperature scaling is performed at time $t = 100n$ ($n = 1, 2, \dots, 10$). From $t = 10^3$ to 10^4 , the momentum autocorrelation function $\langle \mathbf{P}(0) \cdot \mathbf{P}(t) \rangle$

($t = 10^{-3}n$, $n = 0, \dots, 10^4$) is calculated and averaged over the samples, which is used to estimate the exponential decay rate. From $t = 10^4$ to $t = 1.5 \times 10^4$, the correlation functions $\langle \mathbf{P}(0) \cdot \mathbf{P}(t) \rangle$, $\langle \mathbf{P}(0) \cdot \mathbf{F}(t) \rangle$, and $\langle \mathbf{F}(0) \cdot \mathbf{F}(t) \rangle$ ($t = 10^{-4}n$, $n = 0, \dots, 10^4$) are calculated and averaged over the samples. By using those three correlation functions, the Mori memory kernel $K(t)$ and, thus from Eq. (3), the fluctuating force autocorrelation function $\langle \mathbf{F}^+(0) \cdot \mathbf{F}^+(t) \rangle$ are calculated following the procedure described in Ref. [31].

For each set of the simulation parameters, a total of eight samples with different initial solvent configurations are prepared in thermal equilibrium through temperature scaling. For each correlation function $\langle \mathbf{A}(0) \cdot \mathbf{B}(t) \rangle$, we have $\langle A_x(0)B_x(t) \rangle$ and $\langle A_y(0)B_y(t) \rangle$, which are equal to $\frac{1}{2}\langle \mathbf{A}(0) \cdot \mathbf{B}(t) \rangle$. Hence, from $n = 16$ samples, we estimate the value of the correlation function as twice the sample mean, and its standard deviation σ is estimated as

$$\sigma = \frac{2s_n}{\sqrt{n}}, \quad (101)$$

where s_n^2 is the sample variance. The statistical errors of the simulation results are suppressed within 1% of the maximum magnitude of the correlation functions; see Figs. 7, 8, and 12 for the statistical errors of the force autocorrelation functions and Fig. 13 for that of the momentum autocorrelation function.

The effect of the boundary conditions, which are introduced due to the finite size of the MD simulation domain, is also investigated. Some artificial effects may be possible due to

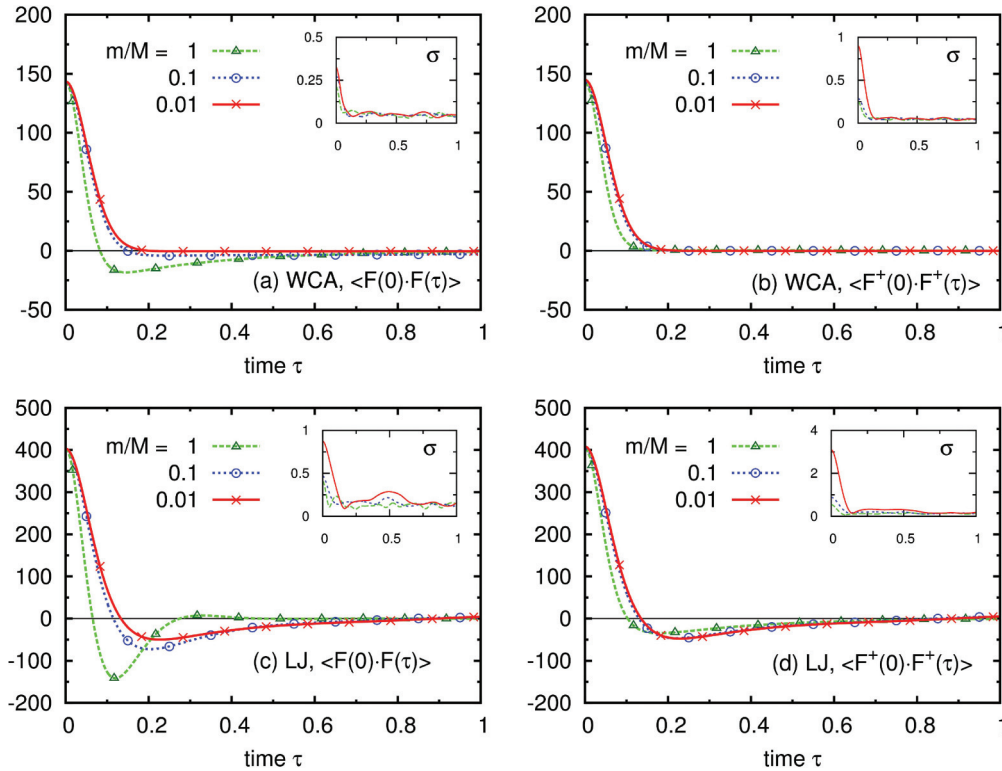


FIG. 7. (Color online) Plots of $\langle \mathbf{F}(0) \cdot \mathbf{F}(\tilde{\tau}) \rangle$ [in panels (a) and (c)] and $\langle \mathbf{F}^+(0) \cdot \mathbf{F}^+(\tilde{\tau}) \rangle$ [in panels (b) and (d)] for various values of the mass ratio m/M from 1 to 0.01. The results are obtained from the MD simulations of the full dynamics under the WCA potential for panels (a) and (b) and under the LJ potential for panels (c) and (d), respectively. The results for $m/M = 0.01$ (depicted by the red solid lines) are chosen as $\langle \mathbf{F}(0) \cdot \mathbf{F}(\tilde{\tau}) \rangle_{\text{NBL}}$ and $\langle \mathbf{F}^+(0) \cdot \mathbf{F}^+(\tilde{\tau}) \rangle_{\text{NBL}}$ and used in the succeeding figures. Note that the microscopic time $\tilde{\tau} = t/\sqrt{m}$ is used and the force autocorrelations are scaled by the number density a of the solvent particles. In the insets, the standard deviation σ is plotted; see Eq. (101).

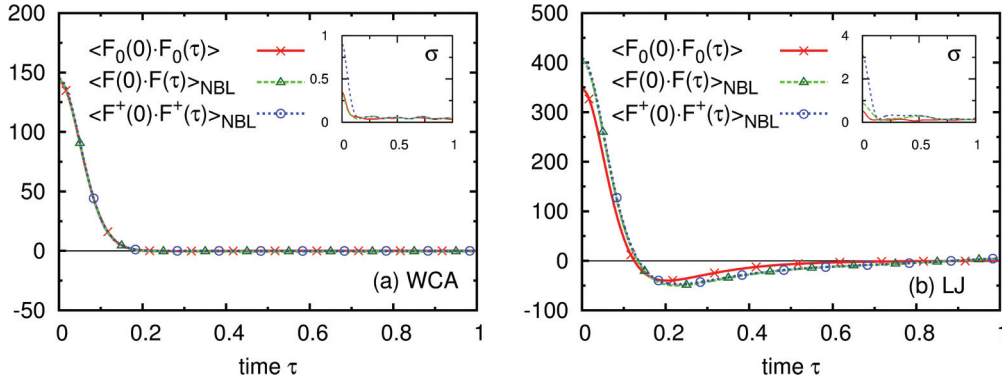


FIG. 8. (Color online) Comparison of $\langle \mathbf{F}(0) \cdot \mathbf{F}(\tilde{\tau}) \rangle_{\text{NBL}}$ and $\langle \mathbf{F}^+(0) \cdot \mathbf{F}^+(\tilde{\tau}) \rangle_{\text{NBL}}$ with $\langle \mathbf{F}_0(0) \cdot \mathbf{F}_0(\tilde{\tau}) \rangle$ obtained from the frozen dynamics MD simulation. The results for the WCA potential are plotted in panel (a) and those for the LJ potential are in panel (b). For $\langle \mathbf{F}(0) \cdot \mathbf{F}(\tilde{\tau}) \rangle_{\text{NBL}}$ and $\langle \mathbf{F}^+(0) \cdot \mathbf{F}^+(\tilde{\tau}) \rangle_{\text{NBL}}$, the full dynamics MD simulation results for $m/M = 0.01$ are plotted. In the insets, the standard deviation σ is plotted.

the possibility that a solvent particle which collided with the Brownian particle can collide again with the Brownian particle after leaving and reentering the domain. Also, two definitions of the number density of the solvent particles (i.e., N/V or N/V^*) may result in different values, unless the volume of the Brownian particle is negligible compared to the volume of the system. To this end, smaller values of the box size L are used and the results are compared. In addition, we impose the reflecting boundary conditions for the frozen dynamics simulations and compare the results to the system with the periodic boundary conditions. Hence, we confirm that such effects are negligible in our MD simulation results.

B. Force autocorrelations

We first observe how the total force autocorrelation function and the fluctuating force autocorrelation function change as the value of m/M is decreasing. In Fig. 7, these autocorrelation functions obtained from the full dynamics MD simulations are plotted for various values of the mass ratio. The microscopic time $\tilde{\tau} = t/\sqrt{m}$ is used. Since the magnitude of the force autocorrelations is proportional to the number density a of the solvent particles, they are also scaled by a . For both interaction potentials, it is clearly observed that $\langle \mathbf{F}(0) \cdot \mathbf{F}(\tilde{\tau}) \rangle$ and $\langle \mathbf{F}^+(0) \cdot \mathbf{F}^+(\tilde{\tau}) \rangle$ converge. By choosing the results for $m/M = 0.01$ as $\langle \mathbf{F}(0) \cdot \mathbf{F}(\tilde{\tau}) \rangle_{\text{NBL}}$ and $\langle \mathbf{F}^+(0) \cdot \mathbf{F}^+(\tilde{\tau}) \rangle_{\text{NBL}}$, the rate of convergence is investigated. For both potentials, the overall deviation

$$\left(\int_0^\infty |\langle \mathbf{F}(0) \cdot \mathbf{F}(\tilde{\tau}) \rangle - \langle \mathbf{F}(0) \cdot \mathbf{F}(\tilde{\tau}) \rangle_{\text{NBL}}|^2 d\tilde{\tau} \right)^{1/2} \quad (102)$$

is decreasing with $O(m/M)$ and the same rate of convergence is observed for the fluctuating force autocorrelation function. For the WCA potential, pointwise convergence of both force autocorrelation functions is clearly observed to be first order in m/M for all times where the force autocorrelation functions have nonzero values. For the LJ potential, clear first-order convergence in m/M is observed for short times $\tilde{\tau} < 0.2$ for $\langle \mathbf{F}(0) \cdot \mathbf{F}(\tilde{\tau}) \rangle$ and $\tilde{\tau} < 0.5$ for $\langle \mathbf{F}^+(0) \cdot \mathbf{F}^+(\tilde{\tau}) \rangle$, respectively. We also observe that although two force autocorrelations eventually converge to the same time profile (see Fig. 8), for the intermediate values of m/M the time profiles of

$\langle \mathbf{F}^+(0) \cdot \mathbf{F}^+(\tilde{\tau}) \rangle$ are much closer to the limiting time profiles than $\langle \mathbf{F}(0) \cdot \mathbf{F}(\tilde{\tau}) \rangle$ for both potentials.

We compare $\langle \mathbf{F}(0) \cdot \mathbf{F}(\tilde{\tau}) \rangle_{\text{NBL}}$ and $\langle \mathbf{F}^+(0) \cdot \mathbf{F}^+(\tilde{\tau}) \rangle_{\text{NBL}}$ with the frozen dynamics autocorrelation function $\langle \mathbf{F}_0(0) \cdot \mathbf{F}_0(\tilde{\tau}) \rangle$ obtained from the frozen dynamics MD simulations in Fig. 8. As expected from Eq. (15), $\langle \mathbf{F}(0) \cdot \mathbf{F}(\tilde{\tau}) \rangle_{\text{NBL}}$ and $\langle \mathbf{F}^+(0) \cdot \mathbf{F}^+(\tilde{\tau}) \rangle_{\text{NBL}}$ coincide for both potentials. On the other hand, $\langle \mathbf{F}_0(0) \cdot \mathbf{F}_0(\tilde{\tau}) \rangle$ coincides with these two functions for the WCA potential, but for the LJ potential there is a clear discrepancy, which results from the initial configuration of the solvent we imposed in the frozen dynamics MD simulation. Since the initial positions of the solvent particles are uniformly distributed *outside* the interaction range, every solvent particle initially has positive total energy and no particle is trapped in the potential well. However, in order that the frozen dynamics correctly describes the full dynamics in the NBL regime, the trapped particles should also be considered. This can be clearly shown by the radial distribution function $g(r)$ of the interparticle distance r between the Brownian particle and a solvent. As shown in Fig. 9, even though identical

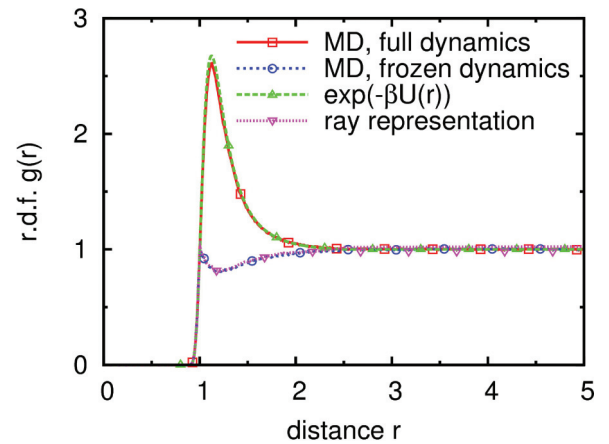


FIG. 9. (Color online) For the full dynamics (with $m/M = 0.01$) and the frozen dynamics MD simulations under the LJ potential, the radial distribution functions $g(r)$ are plotted. The distance r is the interparticle distance between the Brownian particle and a solvent particle. The full dynamics result coincides with $e^{-\beta U(r)}$, while the frozen dynamics result agrees well with the curve calculated from the ray representation approach.

initial conditions are used for the full dynamics and the frozen dynamics simulations, the radial distribution function of the frozen dynamics is quite different from that of the full dynamics in the NBL regime. In the full dynamics, $g(r)$ has the form $e^{-\beta U(r)}$, which indicates that the system is in the equilibrium state. In the frozen dynamics, $g(r)$ has smaller values in the potential well region. This is because there is no contribution from the trapped solvent particles. Since the full dynamics is a many-body problem whereas the frozen dynamics is eventually a set of one-body problems, even if the initial solvent configuration is not in the equilibrium state, the full dynamics attains the equilibrium state by the ergodic postulate but the frozen dynamics may fail to do so. If the initial condition is chosen as described above, the inconsistency between the initial condition and the equilibrium state occurs inside the interaction range. The inconsistency quickly disappears for the WCA potential, but it remains forever for the LJ potential.

Next we compare the time profiles of the frozen dynamics force autocorrelation function $\langle \mathbf{F}_0(0) \cdot \mathbf{F}_0(\tilde{\tau}) \rangle$ obtained by numerical evaluation of the analytic expressions and the frozen dynamics MD simulation. For the numerical evaluation of the ensemble-averaged expression, Eq. (22) is used. The one-particle trajectory $\mathbf{x}(t)$ is calculated by the fourth-order Runge-Kutta method with $m = 1$ and $\Delta t = 10^{-3}$. For the integrations over r and ϕ variables, the trapezoid rule with 10^3 subintervals is used. The integration interval for r is chosen as $[0.7, 2.5]$. Then, for the integration over the u variable, the Gaussian quadrature [32] with density e^{-au^2} ($u > 0$) is employed with 30 quadrature points. Similarly, to numerically evaluate the ray representation expression, Eq. (69), the fourth-order Runge-Kutta method with $m = 1$ and $\Delta t = 10^{-3}$ is used for the calculation of the trajectory $\boldsymbol{\psi}(t)$. Also, the trapezoid rule with 10^3 subintervals is employed for the integration over r and then the Gaussian quadrature with 30 quadrature points is used for the integration over the u variable. Figure 10 shows that the three methods produce identical results for the WCA potential, whereas for the LJ potential the ray representation result and the frozen dynamics MD result coincide but they are different from the ensemble average result. The coincidence of the ray representation result and the frozen dynamics MD

result is explained by the initial configuration of the solvent that is assumed in the ray representation approach to be identical to the one we imposed in the frozen dynamics MD simulation; see Sec. IV E. Hence, the discrepancy between the ray representation result and the ensemble average result is also attributed to no consideration of the trapped particles in the ray representation approach. This can be verified by evaluating the ensemble-averaged expression only over the nontrapped particles. As expected, the resulting time profile coincides with the ray representation result. In addition, we confirm that the radial distribution function obtained from the ray representation approach coincides with that obtained from the frozen dynamics MD simulation; see Fig. 9.

Therefore, we have the following relations of the ensemble-averaged expression, Eq. (20), and the ray representation expression, Eq. (65), of $\langle \mathbf{F}_0(0) \cdot \mathbf{F}_0(\tilde{\tau}) \rangle$ to the fluctuating force autocorrelation function $\langle \mathbf{F}^+(0) \cdot \mathbf{F}^+(\tilde{\tau}) \rangle_{\text{NBL}}$ in the NBL regime.

- (i) For a purely repulsive potential, both expressions produce $\langle \mathbf{F}^+(0) \cdot \mathbf{F}^+(\tilde{\tau}) \rangle_{\text{NBL}}$.
- (ii) For a potential containing an attractive component, the ensemble-averaged expression produces $\langle \mathbf{F}^+(0) \cdot \mathbf{F}^+(\tilde{\tau}) \rangle_{\text{NBL}}$, whereas the ray representation expression produces only the contribution of the nontrapped particles.

We further confirm these by comparing $\langle \mathbf{F}^+(0) \cdot \mathbf{F}^+(\tilde{\tau}) \rangle_{\text{NBL}}$, ensemble-average results over all particles and only over the nontrapped particles, and ray representation results for various values of the potential parameters. Figure 11 shows the results under the LJ potential for various values of ϵ . It is observed that for a larger value of ϵ , the discrepancy between the ensemble averages over all particles and over the trapped particles becomes larger. In other words, the contribution of the trapped particles to $\langle \mathbf{F}^+(0) \cdot \mathbf{F}^+(\tilde{\tau}) \rangle_{\text{NBL}}$ increases as the attractive component of the potential becomes stronger. It is also observed that the contribution of the trapped particles complicates the tail behavior of $\langle \mathbf{F}^+(0) \cdot \mathbf{F}^+(\tilde{\tau}) \rangle_{\text{NBL}}$ with a longer correlation time length.

We also investigate the long-time behavior of the force autocorrelation functions, which is shown in Fig. 12. For the WCA potential, $\langle \mathbf{F}_0(0) \cdot \mathbf{F}_0(\tilde{\tau}) \rangle$ quickly decays to zero without attaining negative values. This can be explained

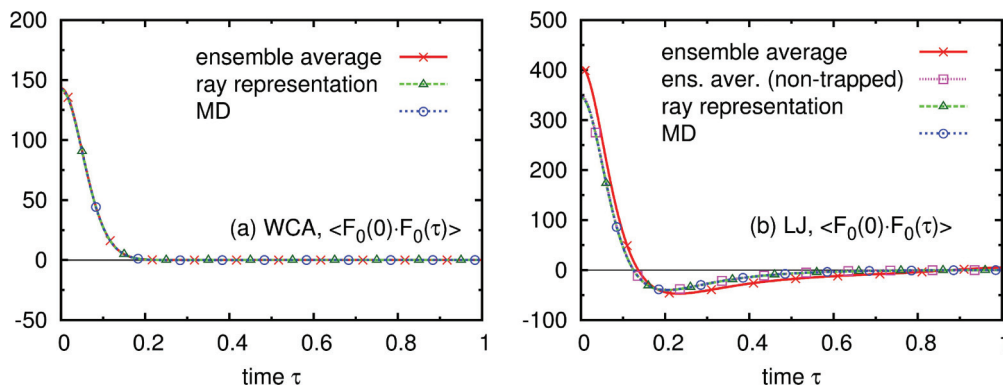


FIG. 10. (Color online) Comparison of the curves of $\langle \mathbf{F}_0(0) \cdot \mathbf{F}_0(\tilde{\tau}) \rangle$ obtained by numerical evaluation of the ensemble-averaged expression [i.e., Eq. (22)], the ray representation expression [i.e., Eq. (69)], and the frozen dynamics MD simulation. The results are shown in panel (a) for the WCA potential and in panel (b) for the LJ potential, respectively. In panel (b), the ensemble average over the nontrapped particles is also plotted.

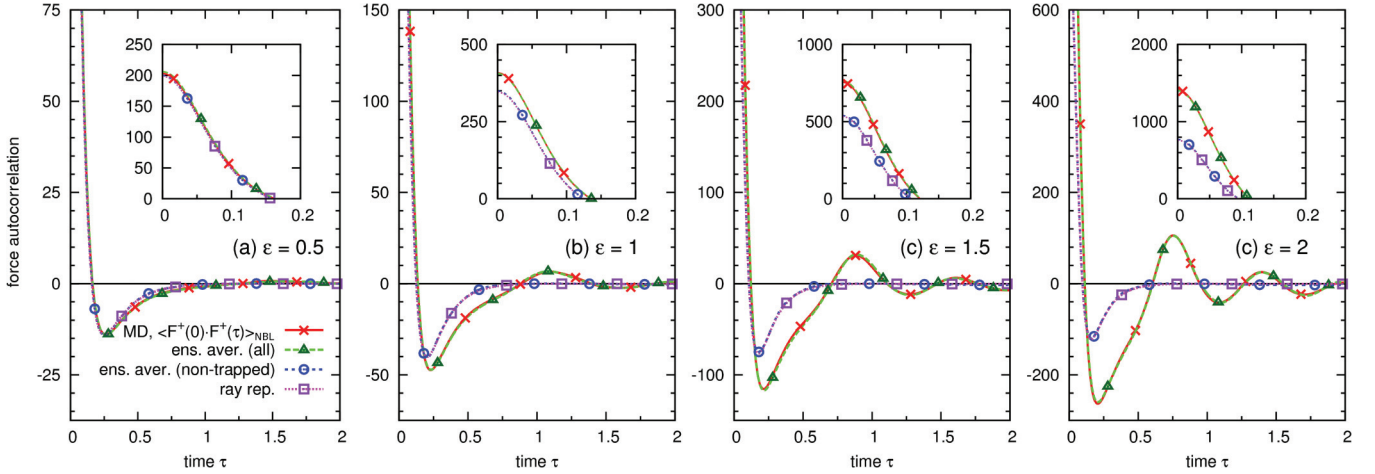


FIG. 11. (Color online) For various values of the ϵ parameter of the LJ potential, $\langle \mathbf{F}^+(0) \cdot \mathbf{F}^+(\tilde{\tau}) \rangle_{\text{NBL}}$ obtained from the full dynamics MD simulation and $\langle \mathbf{F}_0(0) \cdot \mathbf{F}_0(\tilde{\tau}) \rangle$ obtained from the ensemble-averaged expression are compared, and $\langle \mathbf{F}_0(0) \cdot \mathbf{F}_0(\tilde{\tau}) \rangle$ obtained from the ensemble average over the nontrapped particles and $\langle \mathbf{F}_0(0) \cdot \mathbf{F}_0(\tilde{\tau}) \rangle$ obtained from the ray representation expression are also compared. The inverse temperature is fixed as $\beta = 1$. In the insets, positive values of the force autocorrelation functions are plotted for short times.

by the fact that every one-particle trajectory $\mathbf{x}(t)$ under the WCA potential quickly escapes from the interaction range and the two-time force product $\mathbf{f}(\mathbf{x}) \cdot \mathbf{f}(\mathbf{x}(t))$ has non-negative values for all times. The coincidence of $\langle \mathbf{F}^+(0) \cdot \mathbf{F}^+(\tilde{\tau}) \rangle_{\text{NBL}}$ to $\langle \mathbf{F}_0(0) \cdot \mathbf{F}_0(\tilde{\tau}) \rangle$ is observed for all times. On the other hand, although the overall shape of $\langle \mathbf{F}(0) \cdot \mathbf{F}(\tilde{\tau}) \rangle_{\text{NBL}}$ coincides with $\langle \mathbf{F}_0(0) \cdot \mathbf{F}_0(\tilde{\tau}) \rangle$ for short times (see Fig. 8), the total force autocorrelation function has a negative tail, which is expected from Eq. (17). The magnitude of the negative tail, which is proportional to the mass ratio, is negligible to the magnitude at time $\tilde{\tau} = 0$, but due to its existence the time integral of the total force autocorrelation function eventually decays to zero. Similarly, for the LJ potential, we confirm the coincidence of $\langle \mathbf{F}^+(0) \cdot \mathbf{F}^+(\tilde{\tau}) \rangle_{\text{NBL}}$ to $\langle \mathbf{F}_0(0) \cdot \mathbf{F}_0(\tilde{\tau}) \rangle$ for all times and observe that $\langle \mathbf{F}(0) \cdot \mathbf{F}(\tilde{\tau}) \rangle_{\text{NBL}}$ has slightly smaller values than $\langle \mathbf{F}^+(0) \cdot \mathbf{F}^+(\tilde{\tau}) \rangle_{\text{NBL}}$ and $\langle \mathbf{F}_0(0) \cdot \mathbf{F}_0(\tilde{\tau}) \rangle$. In addition, we also compare the ensemble average $\langle \mathbf{F}_0(0) \cdot \mathbf{F}_0(\tilde{\tau}) \rangle$ over the nontrapped particles, the ray representation result, and the frozen dynamics MD simulation. For both potentials,

the three results agree very well for all times, which confirms that the ray representation approach only considers the contribution of the nontrapped particles.

C. Friction coefficient γ

We first estimate the friction coefficient γ from the exponential decay rate of the momentum autocorrelation function of the Brownian particle. Figure 13 shows the time profile of $\langle \mathbf{P}(0) \cdot \mathbf{P}(\tilde{\tau}) \rangle$, which is obtained from the full dynamics MD simulation under the LJ potential with $m/M = 0.01$. In a wide time interval, $\langle \mathbf{P}(0) \cdot \mathbf{P}(\tilde{\tau}) \rangle$ exhibits exponential decay. By using the nonlinear least-squares Marquardt-Levenberg algorithm [32] with the form $c_1 \exp(-c_2 \tilde{\tau})$ for $0 \leq \tilde{\tau} \leq 100$, c_2 is estimated as 5.76×10^{-2} and, from Eq. (7), $m^{-1/2} \gamma$ is estimated as 5.76. From Eq. (101) with $n = 16$ samples, the standard deviation of the estimated value is estimated as $\sigma = 0.10$. The deviation from the exponential decay for short times is expected from the fact that the second derivative of the

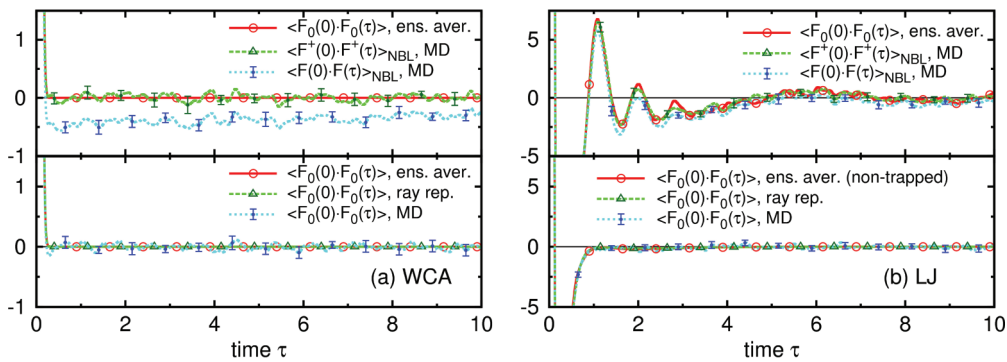


FIG. 12. (Color online) Plots of the tails (i.e., long-time behavior) of the force autocorrelation functions. The results for the WCA potential are plotted in panel (a), whereas those for the LJ potential are in panel (b). In the upper plot of each panel, plotted are $\langle \mathbf{F}_0(0) \cdot \mathbf{F}_0(\tilde{\tau}) \rangle$ [evaluated from the ensemble-averaged expression, Eq. (22)], $\langle \mathbf{F}^+(0) \cdot \mathbf{F}^+(\tilde{\tau}) \rangle_{\text{NBL}}$, and $\langle \mathbf{F}(0) \cdot \mathbf{F}(\tilde{\tau}) \rangle_{\text{NBL}}$ (obtained from the full dynamics MD simulation). In the lower plot, three curves of $\langle \mathbf{F}_0(0) \cdot \mathbf{F}_0(\tilde{\tau}) \rangle$ obtained by the following methods are plotted: numerical evaluation of the ensemble average over the nontrapped particles, numerical evaluation of the ray representation expression, and the frozen dynamics MD simulation. For the MD simulation results, error bars with 2σ are also plotted.

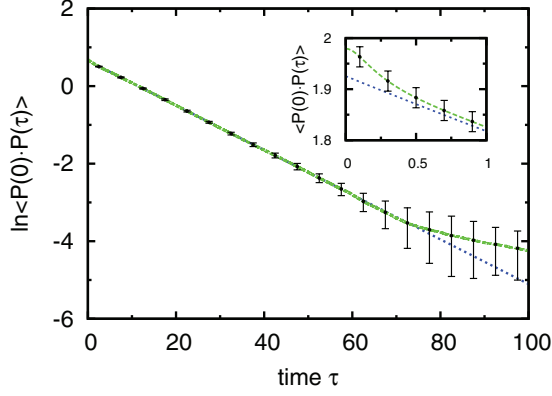


FIG. 13. (Color online) The log plot of the momentum autocorrelation function $\langle \mathbf{P}(0) \cdot \mathbf{P}(\tau) \rangle$. The blue dotted line indicates the straight line $\ln c_1 - c_2 \tau$, where c_1 and c_2 are evaluated from the nonlinear least-squares fitting of $\langle \mathbf{P}(0) \cdot \mathbf{P}(\tau) \rangle$ with the form $c_1 e^{-c_2 \tau}$. Error bars with 2σ are also plotted. Since the magnitude of statistical errors is comparable for all times, the error bars become longer for longer times in the log plot. In the inset, the time profile of $\langle \mathbf{P}(0) \cdot \mathbf{P}(\tau) \rangle$ is plotted with $c_1 e^{-c_2 \tau}$ for short times.

momentum autocorrelation function is equal to the negative of the total force autocorrelation function. Also, the zero slope of $\langle \mathbf{P}(0) \cdot \mathbf{P}(\tau) \rangle$ at $\tau = 0$ is clearly observed. In addition, the initial value of the momentum autocorrelation function is 1.98, which is expected from Eq. (14) with $N = 10^4$ and $m/M = 0.01$. On the other hand, the decay of the momentum autocorrelation function for long times appears to be algebraic.

Next we investigate the following time integrals of the force autocorrelation functions:

$$\gamma^*(\bar{\tau}) = \frac{\beta\sqrt{m}}{d} \int_0^{\bar{\tau}} \langle \mathbf{F}(0) \cdot \mathbf{F}(\bar{s}) \rangle d\bar{s}, \quad (103a)$$

$$\gamma_0(\bar{\tau}) = \frac{\beta\sqrt{m}}{d} \int_0^{\bar{\tau}} \langle \mathbf{F}_0(0) \cdot \mathbf{F}_0(\bar{s}) \rangle d\bar{s}, \quad (103b)$$

$$\gamma^+(\bar{\tau}) = \frac{\beta\sqrt{m}}{d} \int_0^{\bar{\tau}} \langle \mathbf{F}^+(0) \cdot \mathbf{F}^+(\bar{s}) \rangle d\bar{s}. \quad (103c)$$

For $\langle \mathbf{F}_0(0) \cdot \mathbf{F}_0(\bar{\tau}) \rangle$, both the ensemble-averaged expression and the ray representation expression are used and the corresponding time-dependent friction coefficients are denoted by $\gamma_0^{\text{ens}}(\bar{\tau})$ and $\gamma_0^{\text{ray}}(\bar{\tau})$, respectively. In Fig. 14, these time-dependent friction coefficients are plotted for the LJ potential. Although $\gamma^*(\bar{\tau})$ appears similar to $\gamma_0^{\text{ens}}(\bar{\tau})$ and $\gamma^+(\bar{\tau})$ for short times, it eventually decays without attaining a stationary value. On the other hand, $\gamma_0^{\text{ens}}(\bar{\tau})$ and $\gamma^+(\bar{\tau})$ have very similar time profiles and appear to have the same stationary value. Although the time profile of $\gamma_0^{\text{ray}}(\bar{\tau})$ is quite different from that of $\gamma_0^{\text{ens}}(\bar{\tau})$, its stationary value appears to be the same as that of $\gamma_0^{\text{ens}}(\bar{\tau})$. This confirms that the net contribution of trapped solvent particles to the value of γ is zero. However, to determine the precise value of γ from the time integral $\gamma_0^{\text{ens}}(\bar{\tau})$ or $\gamma^+(\bar{\tau})$, $\bar{\tau} = 10$ is rather short, since $\langle \mathbf{F}_0(0) \cdot \mathbf{F}_0(\bar{\tau}) \rangle$ or $\langle \mathbf{F}^+(0) \cdot \mathbf{F}^+(\bar{\tau}) \rangle_{\text{NBL}}$ still attains nonzero oscillating values and the corresponding time integral has also an oscillation, the magnitude of which is not negligible. The value of $m^{-1/2}\gamma$ is roughly estimated as 5.8 ± 0.2 for γ_0^{ens} and γ^+ . On the other hand, $\gamma_0^{\text{ray}}(\bar{\tau})$ attains an almost complete plateau for $\bar{\tau} > 5$ and

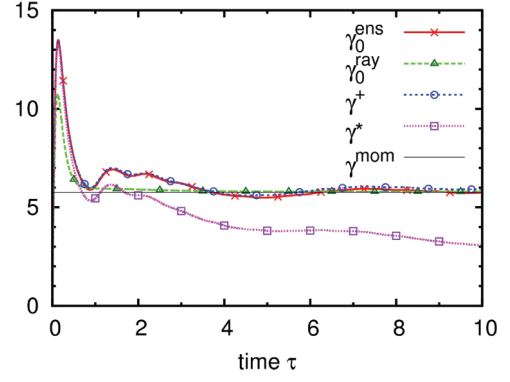


FIG. 14. (Color online) Plotted are the time-dependent friction coefficients $\gamma_0^{\text{ens}}(\bar{\tau})$, $\gamma_0^{\text{ray}}(\bar{\tau})$, $\gamma^+(\bar{\tau})$, and $\gamma^*(\bar{\tau})$, defined in Eq. (103), for the LJ potential. The black horizontal line indicates the value estimated from the exponential decay rate of the momentum autocorrelation function of the Brownian particle for $m/M = 0.01$.

$m^{-1/2}\gamma$ is estimated as 5.79, which is consistent with the value 5.76 with $\sigma = 0.10$, estimated from the exponential decay rate of the momentum autocorrelation function. The time integral $\check{\gamma}_0^{\text{ens}}(\bar{\tau})$ of the ensemble average only over the nontrapped particles [cf. $\gamma_0^{\text{ens}}(\bar{\tau})$] has the same time profile as $\gamma_0^{\text{ray}}(\bar{\tau})$ and hence gives the same value of γ . Note that obtaining γ from $\check{\gamma}_0^{\text{ens}}(\bar{\tau})$ and $\gamma_0^{\text{ray}}(\bar{\tau})$ is equivalent to the evaluation of Eqs. (27) and (71), respectively.

We evaluate the values of γ of the WCA and LJ potentials as a function of ϵ and compare them with the results of the HS interaction and the SqW potential. For $d = 2$, Eqs. (27) and (71) are used for the ensemble-average result and the ray representation result, respectively, which produce identical results. In Fig. 15, the WCA potential result for $\epsilon \leq 3$ with $\beta = 1$ is presented. As ϵ increases, γ also increases. The friction coefficient γ^{WCA} of the WCA potential with $\sigma = 1$ is compared with the friction coefficient γ^{HS} of the HS system. For all values of ϵ , γ^{WCA} is always smaller than γ^{HS} with $R = 2^{1/6}\sigma$. For $\epsilon = 1$, γ^{WCA} is equal to γ^{HS} with $R = 0.972\sigma$. For $\epsilon = 1.9$, γ^{WCA} is equal to γ^{HS} with $R = \sigma$. Similarly, the

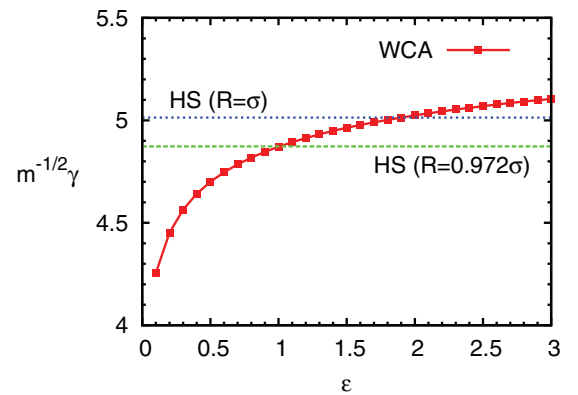


FIG. 15. (Color online) Plot of $m^{-1/2}\gamma$ as a function of the ϵ parameter of the WCA potential. The ray representation expression for $d = 2$, Eq. (71), is used. The other parameters are fixed as $\sigma = 1$, $\beta = 1$, and $a = 1$. The values of γ of the HS system with $R = 0.972\sigma$ and $R = \sigma$ are also plotted by the horizontal lines.

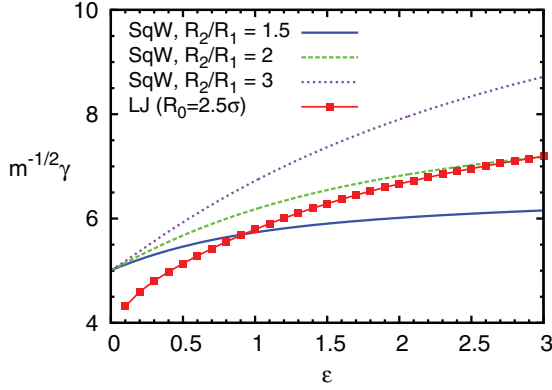


FIG. 16. (Color online) Plot of $m^{-1/2}\gamma$ as a function of the ϵ parameter of the LJ potential. The ray representation expression for $d = 2$, Eq. (71), is used. The other parameters are fixed as $\sigma = 1$, $R_0 = 2.5\sigma$, $\beta = 1$, and $a = 1$. The values of $m^{-1/2}\gamma$ of the SqW system with $\epsilon = 1$, $R_1 = 1$, and different values of R_2 (1.5, 2, and 3) are also plotted by evaluating Eq. (85). Note that as $\epsilon \rightarrow 0$, the value of γ of the SqW system becomes the value for the HS system with $R = R_1$.

LJ potential result is presented and compared with the SqW potential result in Fig. 16.

VII. SUMMARY AND DISCUSSION

For the Rayleigh model, the microscopic theory of Brownian motion has been investigated by analytic methods and extensive MD simulations. For a comprehensive understanding of the model in the NBL regime, four typical interaction potentials (the HS interaction, the SqW potential, and the WCA and LJ potentials) have been considered. The main physical quantities of interest are the asymptotic form of the force autocorrelation function of the Brownian particle in the Brownian limit and the friction coefficient γ in the Langevin equation. As pointed out in [28], we always use the term *asymptotic form* to refer to the Brownian limit rather than to a long-time limit. To investigate these quantities, the ensemble-averaged expressions and the ray representation expressions have been derived and numerically evaluated, and MD simulations of the full dynamics with small mass ratio and of the frozen dynamics have been performed.

The theoretical predictions, which have been numerically confirmed, are summarized as follows. As the mass of the Brownian particle increases, the total force autocorrelation function $\langle \mathbf{F}(0) \cdot \mathbf{F}(t) \rangle$ and the fluctuating force autocorrelation function $\langle \mathbf{F}^+(0) \cdot \mathbf{F}^+(t) \rangle$ have similar time profiles to the frozen dynamics force autocorrelation function $\langle \mathbf{F}_0(0) \cdot \mathbf{F}_0(t) \rangle$ [ensemble average over the bath equilibrium ρ_b in Eq. (13)]. However, the time integral of $\langle \mathbf{F}(0) \cdot \mathbf{F}(t) \rangle$ eventually decays, whereas the time integrals of the other autocorrelation functions have the same nonzero stationary value, which is also equal to the friction coefficient estimated from the exponential decay rate of the momentum autocorrelation function of the Brownian particle. Therefore, the asymptotic form of the force autocorrelation function and the friction coefficient can be obtained from $\langle \mathbf{F}_0(0) \cdot \mathbf{F}_0(t) \rangle$.

We have derived two expressions for $\langle \mathbf{F}_0(0) \cdot \mathbf{F}_0(t) \rangle$, Eqs. (20) and (65), by using ensemble averaging and the ray representation approach, respectively. From the property that the dynamics of each solvent particle is decoupled from those of the other solvent particles in the frozen dynamics of the Rayleigh model, these expressions are given in terms of one-particle trajectory, which enables one to obtain the desired quantity without performing MD simulations. By time integration, the corresponding expressions for γ have been obtained; see Eqs. (26) and (67). For a potential depending only on the interparticle distance, further simplified expressions have also been derived. The ensemble-averaged expressions are reduced to be three-dimensional integrations, whereas the ray representation expressions are to be two-dimensional integrations.

We have shown that the ensemble average and the ray representation approach produce identical results for a purely repulsive potential, and that these results also agree very well with the full dynamics and frozen dynamics MD simulation results. Hence, it has been confirmed that the ray representation approach is valid for an unbounded potential containing no attractive component such as the WCA potential, and it is expected that the analysis performed by Kusuoka and Liang [21] under restrictive assumptions can be extended to this case. From the numerical point of view, among the methods we employed to obtain the asymptotic form of the force autocorrelation function and the friction coefficient, the most efficient and numerically reliable one is the ray representation in this case since each one-particle trajectory needs to be calculated for a short time and only a two-dimensional integration needs to be performed. In addition, a Gaussian quadrature can be used for both integration variables, which enables one to obtain numerically reliable results with a relatively small number of trajectory calculations.

For a potential containing an attractive component such as the LJ potential, however, it has been observed that there is a clear discrepancy between the ensemble-average result and the ray representation result for $\langle \mathbf{F}_0(0) \cdot \mathbf{F}_0(t) \rangle$, and it has been shown that the ray representation only produces the contribution of the nontrapped solvent particles. The initial configuration of the solvent particles which is assumed in the ray representation is that the solvent particles are uniformly distributed outside the interaction range, which is different from the bath equilibrium distribution. Contrary to the purely repulsive potential case in which the difference quickly disappears, the difference remains forever in this case since incoming solvent particles to the interaction range cannot be trapped by the potential and thus the contribution of the trapped particles is still missing. The same problem has been observed when the same initial configuration of the solvent is used for the full dynamics and frozen dynamics MD simulations and the results are compared. These discrepancies are attributed to the fundamental difference between the frozen dynamics and the full dynamics of the Rayleigh model. While the full dynamics always attains the equilibrium distribution by the ergodic postulate, for the frozen dynamics the postulate is no longer valid and thus the equilibrium may fail to be achieved even after a long period of time; also, a time average quantity may be different from the one obtained from the ensemble average depending on the choice of the initial

solvent configuration near the Brownian particle. Hence, for the asymptotic form of the force autocorrelation function, if the interaction potential has an attractive component, the only alternative method to the full dynamics MD simulation would be the numerical evaluation of the ensemble-averaged expression. The frozen dynamics MD simulation method with the initial solvent configuration sampled from the bath equilibrium distribution is not efficient since a single sample cannot represent the bath equilibrium and thus a large number of samples should be run. However, if the precise value of the friction coefficient is the only quantity of interest, which is a quite usual case, the ray representation approach and the frozen dynamics MD simulation method can be employed. Actually, it has been shown that they provide a numerically more reliable value of γ than their alternative methods. This is based on the observation that although the contribution of the trapped particles to the time integral of the force autocorrelation function is zero, it complicates the tail behavior of the force autocorrelation function and prevents the time integral from attaining a stationary value.

Another issue that arises for a potential containing an attractive component is the possible existence of the non-trapped trajectories that revolve around the Brownian particle several times; see Fig. 17. For some initial conditions, the trajectories revolve infinitely many times and slight changes in the initial conditions result in large changes in the momentum change $\Delta\mathbf{p} = \mathbf{p}_\infty - \mathbf{p}$. Hence, $\Delta\mathbf{p}$ oscillates very rapidly as the initial condition approaches these points, and the analytic expressions we have derived may have some problem with these singular points. Since the set of singularities has measure zero and we can find a bound for $\Delta\mathbf{p}$ from the conservation of energy, we can show that all expressions are well-defined even in this case. However, the numerical integration of the expressions should be carefully performed and may need more computation time. For example, the use of a Gaussian quadrature for all integration variables may not be efficient due to the nonsmoothness of the integrand. We note that the SqW potential does not have such complicated trajectories.

Finally, closed-form expressions of γ for the HS interaction and the SqW potential have also been derived. Using these results, it has been analytically confirmed for these potentials that the ray representation approach yields the identical expression of γ to the ensemble average. Although not

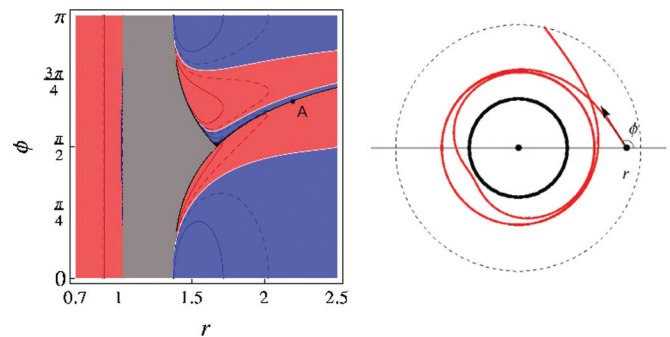


FIG. 17. (Color online) In the left plot, the contour plot of $\lim_{t \rightarrow \infty} \mathbf{f}(\mathbf{x}) \cdot \mathbf{p}(t)$, which appears in Eq. (26), is presented. The initial position \mathbf{x} and the initial momentum \mathbf{p} of the solvent particle are given as $(r, 0)$ and $(u \cos \phi, u \sin \phi)$, respectively, and the value $u = 1$ is used. The gray region indicates the initial values that cause the particle trapped in the potential well forever so that the limit is not defined. The red and blue regions are for positive and negative values of the limit, respectively. The white lines are for the contour with zero value and the red dashed and solid lines are for 0.1 and 0.3, respectively. Similarly, the blue dashed and solid lines are for -0.1 and -0.3 . The black points on the boundary of the gray region and the contour line passing through point A indicate that the trajectories with these initial conditions are still inside the interaction range up to $t = 10$ so that the value of the limit is indecisive from the numerical calculation of trajectories up to $t = 10$. In the right diagram, the trajectory $\mathbf{x}(t)$ with the initial condition designated by point A is plotted until it leaves the interaction range.

included in this paper, expressions for $\langle \mathbf{F}_0(0) \cdot \mathbf{F}_0(t) \rangle$ can also be obtained by following similar procedures performed in Sec. V. For the HS interaction, it can be easily shown that $\langle \mathbf{F}_0(0) \cdot \mathbf{F}_0(t) \rangle = dD\delta(t)$, where $D = 2\beta^{-1}\gamma$. For the SqW potential, it can be shown that the expression for the contribution of the nontrapped particles obtained by ensemble averaging is equal to the expression obtained by the ray representation approach.

ACKNOWLEDGMENTS

This work was partially supported by the new DOE Center on Mathematics for Mesoscopic Modeling of Materials (CM4). Computations were performed at the IBM BG/P with computer time provided by an INCITE grant.

- [1] See, for example, *Focus Issue: Brownian Motion and Diffusion in the 21 Century*, edited by P. Hänggi, J. Łuzka, and P. Talkner [New J. Phys. **7** (2005)] and *Focus Issue: 100 Years of Brownian Motion*, edited by P. Hänggi and F. Marchesoni [Chaos **15** (2005)].
- [2] See, for example, R. Mazo, *Brownian Motion: Fluctuation, Dynamics, and Applications* (Clarendon, Oxford, 2002).
- [3] P. Langevin, C. R. Acad. Sci. (Paris) **146**, 530 (1908); see also D. Lemons and A. Gythiel, *Am. J. Phys.* **65**, 1079 (1997).
- [4] H. Mori, *Prog. Theor. Phys.* **33**, 423 (1965).
- [5] J. Kirkwood, *J. Chem. Phys.* **14**, 180 (1946).
- [6] P. Español and I. Zúñiga, *J. Chem. Phys.* **98**, 574 (1993).
- [7] F. Ould-Kaddour and D. Levesque, *J. Chem. Phys.* **118**, 7888 (2003).
- [8] P. Mazur and I. Oppenheim, *Physica* **50**, 241 (1970).
- [9] G. Kneller and G. Sutmann, *J. Chem. Phys.* **120**, 1667 (2004).
- [10] S.-H. Lee and R. Kapral, *J. Chem. Phys.* **121**, 11163 (2004).
- [11] I. Michaels and I. Oppenheim, *Physica A* **81**, 221 (1975).
- [12] M. Green, *J. Chem. Phys.* **19**, 1036 (1951).
- [13] R. Mazo, *J. Chem. Phys.* **35**, 831 (1961).
- [14] D. Montgomery, *Phys. Fluids* **14**, 2088 (1971).
- [15] R. Mazo, *J. Stat. Phys.* **12**, 427 (1975).
- [16] J. Hynes, *J. Chem. Phys.* **62**, 2972 (1975).

- [17] D. Szász and B. Tóth, *Commun. Math. Phys.* **111**, 41 (1987), and reference as therein.
- [18] D. Dürr, S. Goldstein, and J. Lebowitz, *Commun. Math. Phys.* **78**, 507 (1981).
- [19] D. Dürr, S. Goldstein, and J. Lebowitz, *Z. Wahrsch. verw. Gebiete* **62**, 427 (1983).
- [20] P. Calderoni, D. Dürr, and S. Kusuoka, *J. Stat. Phys.* **55**, 649 (1989).
- [21] S. Kusuoka and S. Liang, *Rev. Math. Phys.* **22**, 733 (2010).
- [22] A. Plyukhin and J. Schofield, *Phys. Rev. E* **68**, 041107 (2003); **69**, 021112 (2004).
- [23] T. Munakata and H. Ogawa, *Phys. Rev. E* **64**, 036119 (2001); M. Uranagase and T. Munakata, *ibid.* **75**, 011110 (2007).
- [24] M. Mansour, A. Garcia, and F. Baras, *Phys. Rev. E* **73**, 016121 (2006).
- [25] M. Cencini, L. Palatella, S. Pigolotti, and A. Vulpiani, *Phys. Rev. E* **76**, 051103 (2007).
- [26] A. Fruleux, R. Kawai, and K. Sekimoto, *Phys. Rev. Lett.* **108**, 160601 (2012).
- [27] B. Nowakowski, *Phys. Rev. E* **53**, 2964 (1996).
- [28] In this paper, we use the term *asymptotic form* (of a force autocorrelation function) only to refer to the Brownian limit $m \ll M$ and not to refer to a long-time limit.
- [29] H. Grabert, *Projection Operator Techniques in Nonequilibrium Statistical Mechanics* (Springer-Verlag, Berlin, 1982).
- [30] J. Hynes, R. Kapral, and M. Weinberg, *Physica A* **80**, 105 (1975).
- [31] H.-K. Shin, C. Kim, P. Talkner, and E.-K. Lee, *Chem. Phys.* **375**, 316 (2010).
- [32] W. Press, S. Teukolsky, W. Vetterling, and B. Flannery, *Numerical Recipes: The Art of Scientific Computing*, 3rd ed. (Cambridge University Press, New York, 2007).